Energetics and Stability of NiMnCo (NMC) Cathode Materials

by

William James Kanitz

A Thesis Presented in Partial Fulfillment
of the Requirements for the Degree
Master of Science

Approved April 2023 by the
Graduate Supervisory Committee:

Alexandra Navrotsky, Chair
Candace Chan
Hongwu Xu

ARIZONA STATE UNIVERSITY

May 2023

ABSTRACT

Lithium nickel manganese cobalt oxides (NMCs) are layered oxide cathode materials which are becoming increasingly popular as the demand for lithium-ion batteries increases. Lithium-ion batteries are used to power modern vehicles and for other battery applications. To better understand the structure and energetics of NMCs, various molar ratios of these compounds were synthesized via a sol-gel method and characterized with powder X-ray diffraction profile fitting. Lattice constants for the nickel, manganese, and cobalt solid solutions were determined. High temperature oxide melt solution calorimetry was used to determine the enthalpies of formation and mixing. All but Li_2MnO_3 had the same space group as $LiCoO_2$ (R-3m). The lattice constants approximately followed a linear fit with cobalt mole fraction ($R^2_{average}$= 0.973) for the cobalt series. As the molar ratio of cobalt increased the lattice constants decreased. The nickel series was less linear ($R^2_{average}$=0.733) and had an opposite lattice constant trend to cobalt. The manganese series possessed a roughly linear trend when excluding the outlier Li_2MnO_3 ($R^2_{average}$=0.282). The formation enthalpy of the cobalt series becomes more negative as more cobalt is added. A second order polynomial fit could be used to model the enthalpies of mixing for the series. NMC2.5,2.5,5 exhibited the most stable energetics. A third order polynomial fit could be used to model the enthalpy of mixing for the nickel and manganese series with NMC811 and NMC181 exhibiting the most stable energetics.

ACKNOWLEDGMENTS

I would like to thank all of my family for their love and support throughout my graduate school journey.

I would especially like to thank Tamilarasan Subramani and Alexandra Navrotsky for their guidance, patience, and assistance with me on this thesis.

I would like to thank all the other members of MOTU for their help and advice along the way none of this would have been possible without them.

TABLE OF CONTENTS

Page

LIST OF TABLES

LIST OF FIGURES

Figure Page

CHAPTER 1

INTRODUCTION

NMC ($LiNi_{1-x}Mn_{1-y}Co_{1-z}O_2$) cathodes are composed of various molar amounts of Ni, Mn, and Co and have numerous applications. As the modern world shifts from petroleum powered vehicles to electric ones, the demand for reliable, powerful, and safe batteries will continue to increase. This family of cathodes has applications for electric

Table 6.1 Typical Cell Chemistries, Cell and Battery Sizes for Different Applications

Application	Cathode Chemistry	Cell Size (Ah)	Battery Voltage (V)	Energy Content (Wh)
Cell Phone	LCO, NMC	2–4	4 (Single cell)	8–16
Laptop	LCO, NMC, NCA	3–4	8–16	24–60
Hybrid Electric Vehicles	NMC, NCA, LMO, LFP	4–30	48–150	500–15,000
Electric Vehicles	NMC, NCA, LMO, LFP	4–80	300–800	15,000–100,000
Commercial Vehicles	LFP, NMC	40–80	400–800	100,000–400,000
PV-Home Storage	NMC, NCA, LMO, LFP	4–40	100–200	3000–10,000
Industrial Storage	NMC, LFP	20–80	200–800	100,000–500,000
Grid Storage	NMC, LFP	60–80	800	2,000,000–30,000,000

Figure 1-Examples of Battery Applications, Including Cathode Chemistry, the Cell Size, the Battery Voltage, and the Energy Content Adopted from Garche et. al[20]

cars and large grid level energy storage. They are also used to energize power tools, e-bikes, and other powertrains. This versatility makes them a popular choice in the changing modern world and a promising prospect for future batteries.[11?] Many of these applications can be seen in Figure 1. Sony Energytec commercialized the first Li-ion battery equipped with a $LiCoO_2$ cathode element in 1990.[2] This battery is still used for portable applications but is insufficient for applications demanding more power, such as electric and hybrid vehicles, mainly for safety reasons.[2]

Rechargeable lithium-ion batteries (LiBs) are a major focus of modern technology due to their high electrochemical storage capabilities and stability. Rechargeable LiBs

have three major components. The first two are the electrodes, a cathode typically containing cobalt and/or manganese and an anode such as a layered lithium transition metal oxide ($LiCoO_2$, or Ni, Mn, Al doped analogues). The third component is the electrolyte which separates the two electrodes. Upon charging, the lithium ions diffuse across the electrolyte from the oxide electrode (cathode) to the graphite electrode

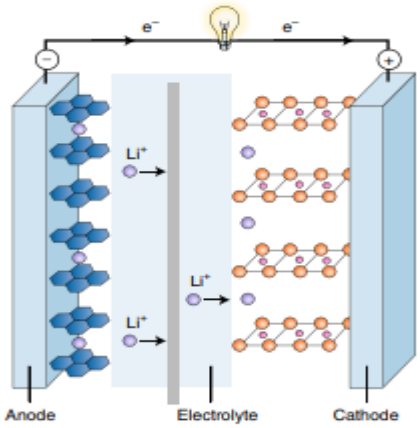

Figure 2 A LiB Cell Containing an Anode, Cathode, and Electrolyte Adopted from Goodenough[10]

(anode).[1] This process is illustrated in Figure 2.

Cobalt-based cathodes are preferred as they have high specific heat, high volumetric capacity, low self-discharge, high discharge voltage, and good cycling performance. Cobalt-based cathodes, however, possess low thermal stability, which is a big disadvantage. Another drawback is that cobalt is mined mainly in Africa, which, due to general social and political instability, makes its availability and price subject to fluctuations. Still, cobalt-based cathodes are the most common. However, other materials are being investigated with the goal of lowering costs and improving cell life. Although there are numerous proposed types of cathodes, our focus will be on NMC cathodes which have the general formula $LiNi_{1-x}Mn_{1-y}Co_{1-z}O_2$ and are a part of the family of lamellar compounds that includes $LiCoO_2$.[2] Typically for these compounds, y and z are

the same and x+y+z=1. Ni is used in the cathode as the electron donor. The cobalt is added to stabilize the Ni^{2+} on the Li^{+} surface by allowing the nickel to avoid any antisite defects that emerge from Li^{+} and Ni^{2+} interactions.[2] Mn is employed to aid in the ordering of the unstable Li^{+} surface.[2]

NMC battery traits vary depending on the molar ratios of Ni, Mn, and Co. In general, increasing the nickel content causes an increase in the energy output of layered oxide cathodes.[3] The increase in Ni also means more Co will likely be necessary to keep the cathode stable.[3] Despite problems with availability, cost, and toxicity, the demand for cobalt continues to increase as LiBs are increasingly common.[8]

Prior experiments have determined the voltage discharge and the capacity of the cell.[2] These experiments typically involved a 1-1-1 ratio of Ni-Mn-Co ($LiNi_{0.33}Mn_{0.33}Co_{0.33}O_2$) which is the standard NMC composition used for current applications. The electronic conductivity is affected by the structural disorder. NMCs show an increase of conductivity when the calcination temperature used in synthesis increases from 800 to 1000 °C, improving the crystallinity of the material.

The hypothesis for this thesis is that as the ratios of Ni/Mn/Co change, the heat of formation will change as the crystal structure and composition vary. This thermodynamic data will be useful for future calculations of phase stability and compatibility involving these materials.

In this thesis, I study the thermodynamic properties of $LiNi_xMn_yCo_zO_2$ NMC cathodes using high temperature oxide melt solution calorimetry. In my experimentation I vary the concentrations of nickel, manganese, and cobalt in NMCs. There are three total systems studied: a nickel series, involving varying amounts of nickel from zero to one

mole fraction with an interval of 0.2 for each solid solution including the 0.5 molar amount; a manganese series with the same mole fractions as nickel; and a cobalt series following the same pattern. In each solid solution, the other two elements in the series possess equimolar amounts with the total molar amount of Ni, Mn, and Co adding to one. This leads to a series of five different materials along with two parent compounds. For example, in the nickel series, $LiNi_{0.8}Mn_{0.1}Co_{0.1}O_{2,}$ (NMC811) is the first compound made in the nickel series, it then follows that NMCs (622), (5,2.5,2.5), (433), (244) are then made. Analogous syntheses follow for the manganese and cobalt series. Parent compounds or end members of these series are also made. The end members are $LiNiO_2$, $LiMnO_2$, $LiCoO_2$, $LiMn_{0.5}Co_{0.5}O_2$, $LiNi_{0.5}Co_{0.5}O_2$, and $LiNi_{0.5}Mn_{0.5}O_2$. The energetics, i.e. enthalpies of formation, of the materials is the primary focus of this thesis.

This investigation proceeds through three major steps: synthesis, characterization, and calorimetry. The first step in synthesis is a thermal decomposition reaction of the three starting materials used: $Ni(II)(NO_3)_2{*}6H_2O$, $Co(II)(NO_3)_2{*}6H_2O$, and $Mn(II)(NO_3)_2{*}4H_2O$. The decomposition reaction determines, using weight loss measurements, the water content of the nitrates, allowing assessment of the quality and purity of the starting materials. This is important because it ensures the correct molar ratios are achieved when synthesizing the final product.

Following the decomposition reaction, solid state synthesis is done. In general, this is a two-step process with the first step being the mixing of all the nitrate components in a crucible with water until they dissolve to ensure good mixing. This crucible is then dried on a hot plate at 80 °C until all the water has evaporated. Next the mixture is heated in the furnace where the nitrates dissociate and the reaction to form the various NMC

compounds occurs. This step is done with slow heating and cooling rates to ensure ample time for the compound to not only form but also to create its proper structure. The end members are synthesized first followed by a nickel series, then manganese, and lastly cobalt. After the synthesis of each compound, powder X-ray diffraction (PXRD) using a Bruker D2 powder diffractometer is run to analyze the structure and characterize the compound. Lastly, oxide melt solution calorimetry is conducted to analyze the energetics of the compounds. The results are then discussed, and conclusions drawn.

The experiments ultimately tell how varying the amounts of nickel, manganese, and cobalt affects the thermodynamic properties of NMCs. The results of this study can be applied in the future to electrochemical testing. Such testing can explore the balance between stability and electrical properties.

CHAPTER 2

EXPERIMENTAL METHODS

I. Decomposition of nitrates

The decomposition reaction is critical for determining the water content of the nitrates ($Ni(NO_3)_2$, $Mn(NO_3)_2$, $Co(NO_3)_2$) the values let us know if the starting samples are pure. Accurate mole percents can be obtained after knowing the water content of the nitrates. The process for decomposition and their reaction temperatures have been well documented[5,6,7].

The decomposition of nickel nitrate hexahydrate ($Ni(NO_3)_2{*}6H_2O$) can be described by the sequential reaction[5]:

$$Ni(NO_3)_2 * 6H_2O \rightarrow Ni(NO_3)_2 * 4H_2O \rightarrow Ni(NO_3)_2 * 3H_2O \rightarrow xNi(NO_3)_2 * yNi(OH)_2 * zH_2O \rightarrow NiO \quad (1)$$

$Ni(NO_3)_2{*}6H_2O$, was heated in air at 700 °C for 8 hours to obtain NiO[5], confirmed by the equation:

$$1 - \frac{Final\ Mass}{Initial\ Mass} * 100 = \%\ Loss\ of\ mass \quad (2)$$

Heating resulted in a 74.55 % loss of mass compared to the theoretical value of 74.32 %. These values are the same within experimental error and no further adjustments in molecular weight need to be made when weighing $Ni(NO_3)_2{*}6H_2O$ later in the synthesis.

The following decomposition reactions were used for the other nitrates

$$Mn(NO_3)_2 * 4H_2O \rightarrow Mn(NO_3)_2 * 2H_2O \rightarrow Mn(NO_3)_2 \rightarrow MnONO_3 \rightarrow MnO_2 \rightarrow$$

$$\frac{1}{2}Mn_2O_3 \rightarrow \frac{1}{3}Mn_3O_4{}^{7} \quad (3)$$

and

$$Co(NO_3)_2 * 6H_2O \rightarrow Co(NO_3)_2 * H_2O \rightarrow \frac{1}{2}Co_2O_3 \rightarrow \frac{1}{3}Co_3O_4 \ {}^{6,19}$$

$$Co(NO_3)_2 * 6H_2O \quad (4)$$

was heated in an alumina crucible to 650 °C at 2 °C/min to produce Co_3O_4 as described in the literature.[6] 72.2 % loss of mass was found compared with a theoretical loss of 72.4 %. $Mn(NO_3)_2{*}4H_2O$ was heated to 1050 °C at 5 °C/min to produce Mn_3O_4.[7] This resulted in a mass loss of 69.9 % with a theoretical loss of 69.6 %. All samples were pure phase as determined by XRD.

II. Synthesis/XRD

Synthesis of the solid solutions was completed by a sol-gel method.[5] Samples were synthesized from $LiNO_3$, $Ni(NO_3)_2{*}6H_2O$, $Mn(NO_3)_2{*}H_2O$, and $Co(NO_3)_2{*}6H_2O$ in stoichiometric proportions to achieve the desired final molar ratio. These materials were mixed in a beaker with water to make a homogenous solution. The beaker was placed on a hot plate at 80 °C to dry. The resulting gel was heated in air in a muffle furnace at 720 °C for 12 hours. Then the material was crushed into a powder for XRD. The following reactions describe the formation of the nickel, manganese, and cobalt solid solutions respectively:

$$LiNO_3 + (1-x)Ni(NO_3)_2 + \left(\frac{x}{2}\right)Mn(NO_3)_2 + \left(\frac{x}{2}\right)Co(NO_3)_2 \rightarrow$$

$$LiNi_{1-x}Mn_{x/2}Co_{x/2}O_2 \quad (5.1)$$

$$LiNO_3 + \left(\frac{x}{2}\right) Ni(NO_3)_2 + (1-x)Mn(NO_3)_2 + \left(\frac{x}{2}\right) Co(NO_3)_2 \rightarrow$$

$$LiNi_{x/2}Mn_{1-x}Co_{x/2}O_2 \quad (5.2)$$

$$LiNO_3 + \left(\frac{x}{2}\right) Ni(NO_3)_2 + \left(\frac{x}{2}\right) Mn(NO_3)_2 + (1-x)Co(NO_3)_2 \rightarrow$$

$$LiNi_{x/2}Mn_{x/2}Co_{1-x}O_2 \quad (5.3)$$

End member compounds were synthesized as follows: Li_2MnO_3 was synthesized by heating the gel at 900 °C for 18 hours. $LiCoO_2$ gel was heated to 700 °C for 1 hour at 10 °C/min and cooled at 10 °C/min. $LiNiO_2$ was synthesized from heating the gel at 720 °C for 18 hours.

Powder X-ray diffraction patterns (PXRD) were obtained using a Bruker D2 X-Ray diffractometer with Cu K_α radiation in the 10-100 ° 2θ range. Initial pure phases were checked with a 1-hour scan and a 12-hour scan with 10-100 ° 2θ was used for profile fitting. The $LiCoO_2$ structure was used as a basis for profile fitting as this structure is well documented and stable. GSAS-II software[14] was used to refine the lattice constants and volumes of the unit cell.

III. Calorimetry

High temperature oxide melt solution calorimetry was conducted in Setaram AlexSYS Tian Calvet twin calorimeters.[12,13] Sample pellets of about 5mg in size were dropped into molten sodium molybdate, $3Na_2O*4MoO_3$, molten solvent at 800 °C. Flushing and bubbling with oxygen was used to control oxygen fugacity, support the dissolution of the compounds and prevent local saturation in the molten salt. The procedure is well documented and described in detail.[12,13] Established values for the heats

of solution of Li_2O, CoO, NiO, Mn_2O_3, O_2 at 800 °C[5,16,17] were used to calculate the heats of formation at 25 °C.

CHAPTER 3

RESULTS AND DISCUSSION

I. Structure and Unit Cell Parameters

XRD revealed the structure of almost all the solid solutions had a rhombohedral structure, possessed hexagonal symmetry, and were space group R-3m. The lattice parameters obtained for $LiCoO_2$ agreed with literature values[5] and the profile fitting values were based on this scan. The only compound not having this structure was Li_2MnO_3, which had the space group C 2/m. This gave it another distinct lattice constant not seen in the R-3m space group as $a \neq b \neq c$. All structures are layered oxides with varying amounts of ordering. The degree of order was not studied further.

In the cobalt series, as the amount cobalt decreased *a*, *c*, and the volume of the unit cell increased linearly, see Fig. 3 and Table 1.

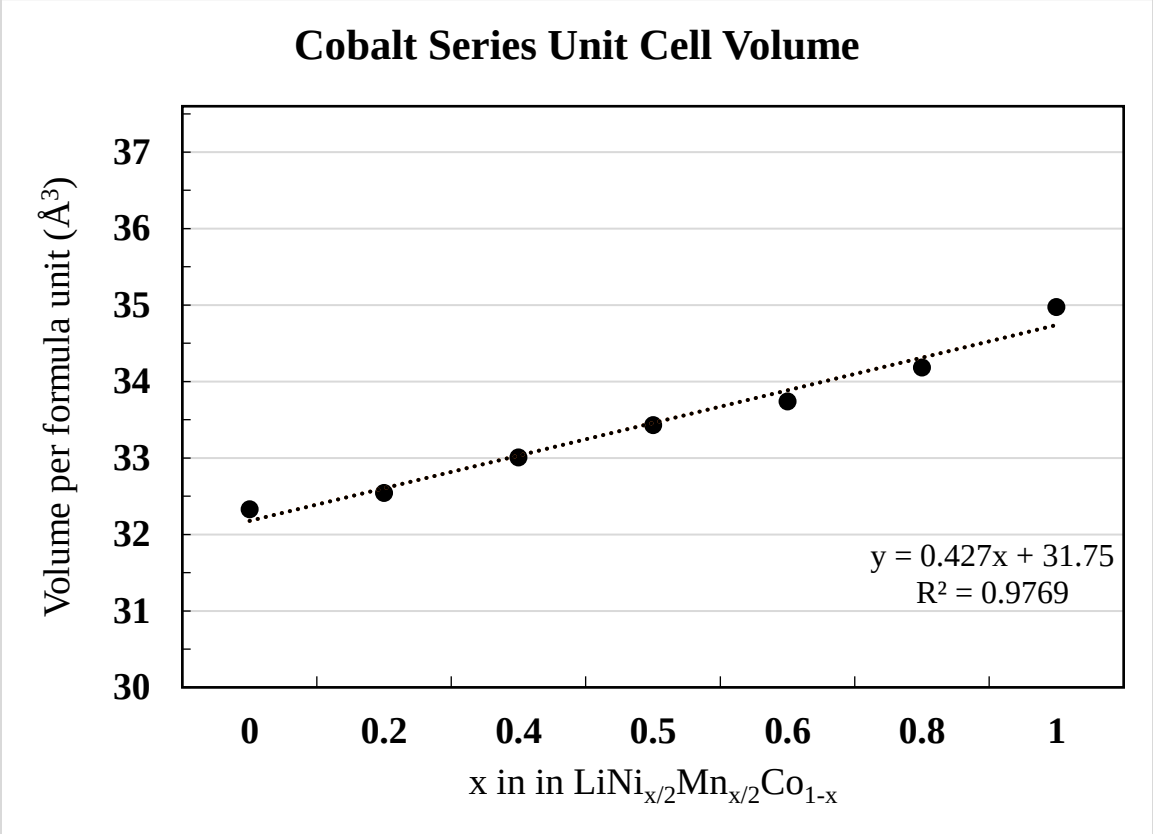

Figure 3: Cobalt Unit Cell Volumetric Trend

The opposite trend was seen in the nickel series (see Fig. 4 and Table 2): as nickel concentration decreases the lattice constants and volume also decreases.

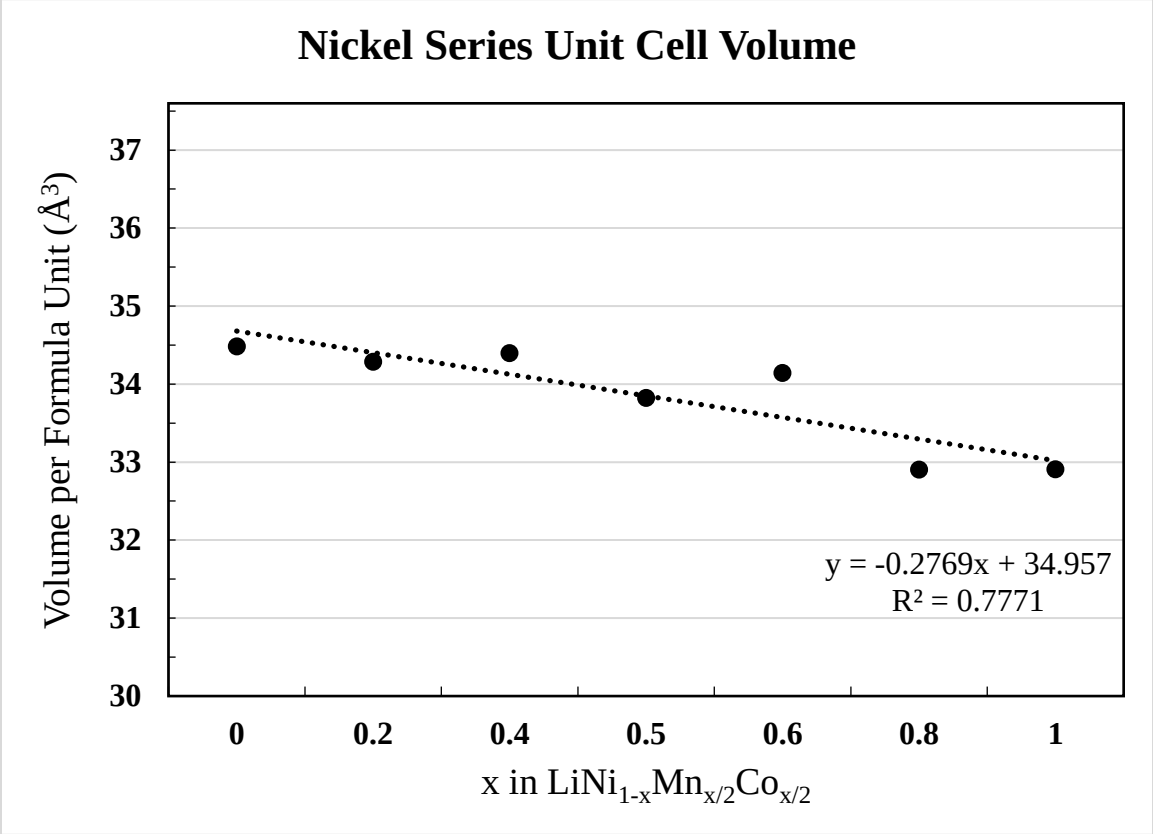

Figure 4 Nickel Series Unit Cell Volumetric Trend

In the manganese series, see Fig. 5 and Table 3, as the amount of manganese decreases, the unit cell volume is roughly constant but may show some scatter at high x

values.

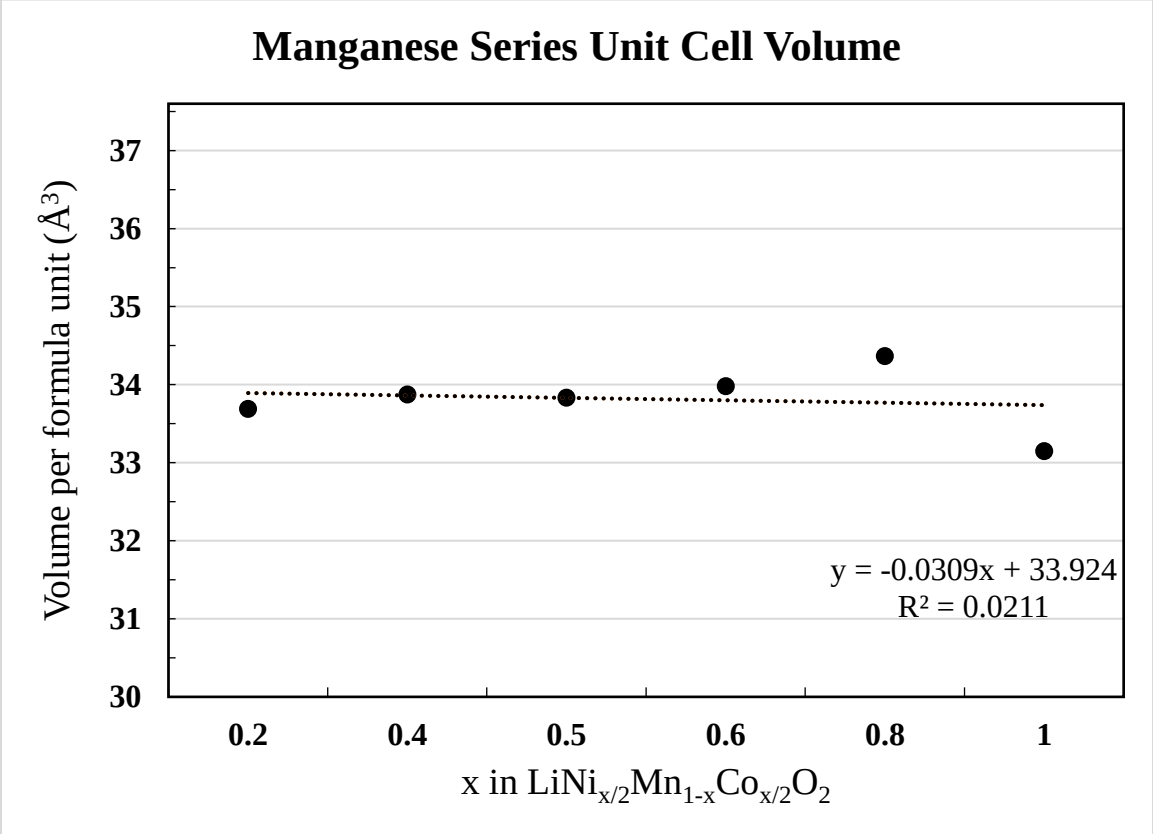

Figure 5 Manganese Unit Cell Volumetric Trend

Li_2MnO_3 is an outlier due to its different space group. It has been omitted from Figure 5 to observe the trend of the solid solutions with the R-3m space group. Lattice parameters *a*, and *c* trends for all series can be found in the appendices. The lattice constant difference is due to the ionic size differences of cobalt, nickel, and in manganese. The octahedral (VI) coordination of these layered oxides have high spin energy splitting which causes different ionic radii. A higher spin leads to a higher ionic radius. Nickel with 6 coordination can either be Ni^{2+} or Ni^{3+} with ionic radii of 0.69 and 0.6 Å respectively.[15] Manganese can either be Mn^{3+} or Mn^{4+} with radii of 0.695 Å and 0.53 Å respectively.[15] Cobalt with 6 coordination is Co^{3+} and has a radius of 0.61 Å.[15]

The size differences occur from the varying ratios of Ni^{2+} paired with Mn^{4+} and Ni^{3+} with Mn^{3+}.

For cobalt the value of *a* increased starting at 2.82 Å and ending at 2.90 Å. For nickel *a* decreased from 2.895 Å to 2.854 Å with a low of 2.853 Å. In the manganese series *a* ran from 2.877-2.875Å with a low 2.873Å.

Table 1 Cobalt Series Unit Cell Parameters

Molar Ratio (x)	Constant *a* (Å)	Constant *c* (Å)	Volume ($Å^3$)
$LiCoO_2$ (0)	2.821±0.001	14.07±0.001	32.328±0.01
NMC118 (0.2)	2.827±0.001	14.108±0.001	32.543±0.007
NMC226 (0.4)	2.843±0.001	14.144±0.001	33.005±0.016
NMC2.5,2.5,5 (0.5)	2.854±0.001	14.216±0.001	33.432±0.016
NMC334 (0.6)	2.863±0.001	14.264±0.001	33.742±0.01
NMC442 (0.8)	2.880±0.001	14.275±0.001	34.183±0.018
$LiNi_{0.5}Mn_{0.5}O_2$ (1)	2.902±0.001	14.389±0.001	34.974±0.018

Table 2: Nickel Series Unit Cell Parameters

Molar Ratio (x)	Constant *a* (Å)	Constant *c* (Å)	Volume ($Å^3$)
$LiNiO_2$ (0)	2.895±0.001	14.251±0.001	34.483±0.01
NMC811 (0.2)	2.890±0.001	14.22±0.002	34.287±0.03
NMC622 (0.4)	2.888±0.001	14.289±0.003	34.398±0.048
NMC5,2.5,2.5 (0.5)	2.878±0.001	14.148±0.002	33.823±0.035
NMC433 (0.6)	2.875±0.001	14.300±0.001	34.141±0.016

NMC244 (0.8)	2.853±0.001	14.006±0.002	32.905±0.03
$LiMn_{0.5}Co_{0.5}O_2$ (1)	2.854±0.001	14.000±0.002	32.906±0.016

Table 3: Manganese Series Unit Cell Parameters

Molar Ratio (x)	Constant *a* (Å)	Constant *c* (Å)	Volume ($Å^3$)
Li_2MnO_3 (0)	4.933±0.005	5.028±0.004	50.011±0.01
NMC181 (0.2)	2.877±0.001	14.092±0.001	33.689±0.01
NMC262 (0.4)	2.877±0.001	14.18±0.001	33.874±0.011
NMC2.5,5,2.5 (0.5)	2.873±0.001	14.200±0.001	33.835±0.016
NMC343 (0.6)	2.874±0.001	14.253±0.001	33.982±0.001
NMC424 (0.8)	2.873±0.001	14.418±0.002	34.365±0.031
$LiNi_{0.5}Co_{0.5}O_2$ (1)	2.850±0.001	14.149±0.004	33.148±0.03

II. Calorimetry

The enthalpies of formation were determined via the enthalpies of drop solution shown in Table 4 which were the literature values for these compounds[16,17,18]

Table 4- Enthalpies of Drop Solution at 800 °C for ΔH_{FE} Calculations

Reactions	ΔH (kJ/mol)
$Li_2O(25°C) \rightarrow Li_2O(dissolved, 800° C)$	ΔH_1=-78.32±3.28
$CoO(25°C) \rightarrow CoO(dissolved,800°C)$	ΔH_2=21.92±0.36
$NiO(25°C) \rightarrow NiO(dissolved,800°C)$	ΔH_3=42.77±0.35
$Mn_2O_3(25°C) \rightarrow Mn_2O_3(dissolved,800°C)$	ΔH_4=175.79±1.38

$O_2(25°C) \rightarrow O_2$ (gas, 800°C) ΔH_5=23.21

To determine the values of the heats of formation, these values were multiplied by the number of moles of each element present in the solid solution. For example: $LiNi_{0.1}Mn_{0.1}Co_{0.8}O_2$ would be calculated by:

$$0.5\Delta H_1 + 0.1\Delta H_3 + 0.05\Delta H_4 + 0.8\Delta H_2 + 0.225\Delta H_5 - H_{DS} = H_{FE}$$

where H_{DS} is the enthalpy of drop solution for NMC118 at 800 °C.

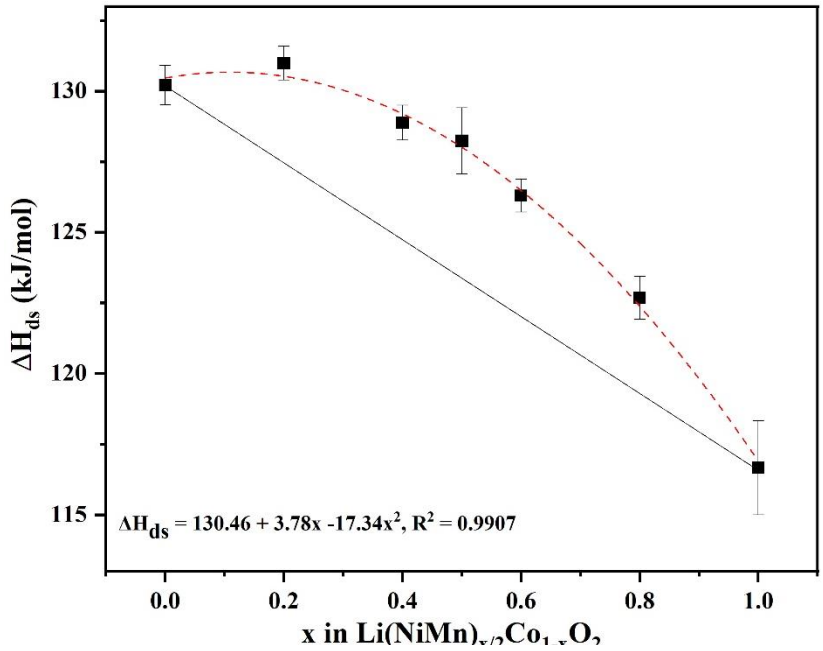

Figure 6 Enthalpy of Drop Solution of the Cobalt Series

As seen in Table 5 and Figure 6, the heats of drop solution ranged from 130.21±0.7 kJ/mol for $LiCoO_2$ to 116.66±1.67 kJ/mol for $LiNi_{0.5}Mn_{0.5}O_2$. The heats of formation ranged from -141.648 to -87.586 kJ/mol for $LiCoO_2$ and $LiNi_{0.5}Mn_{0.5}O_2$ respectively. There is a negative enthalpy of formation for all solid solutions in this series. These values can be fit with a second order polynomial. The fit is relatively ideal and not outside the uncertainties associated with this data.

Table 5

Enthalpies of Drop Solution at 800 °C, Enthalpies of Formation at 25 °C, and Enthalpies of Mixing at 25 °C

Sample	H_{DS} (kJ/mol)	H_{FE} (kJ/mol)	H_{mix} (kJ/mol)
$LiNi_{0.5}Mn_{0.5}O_2$	116.66±1.67 (n)	-87.586±2.37	0±0
$LiNi_{0.4}Mn_{0.4}Co_{0.2}O_2$	122.68±0.76	-101.709±1.84	-3.31±1.54
$LiNi_{0.3}Mn_{0.3}Co_{0.4}O_2$	126.3±0.58	-113.431±1.84	-4.22±1.19
$LiNi_{0.25}Mn_{0.25}Co_{0.5}O_2$	128.24±1.17	-119.422±2.04	-4.805±1.48
$LiNi_{0.2}Mn_{0.2}Co_{0.6}O_2$	128.88±0.62	-124.113±1.77	-4.09±1.00
$LiNi_{0.1}Mn_{0.1}Co_{0.8}O_2$	130.99±0.6	-134.325±1.77	-3.49±0.89
$LiCoO_2$	130.21±0.7	-141.648±1.82	0±0

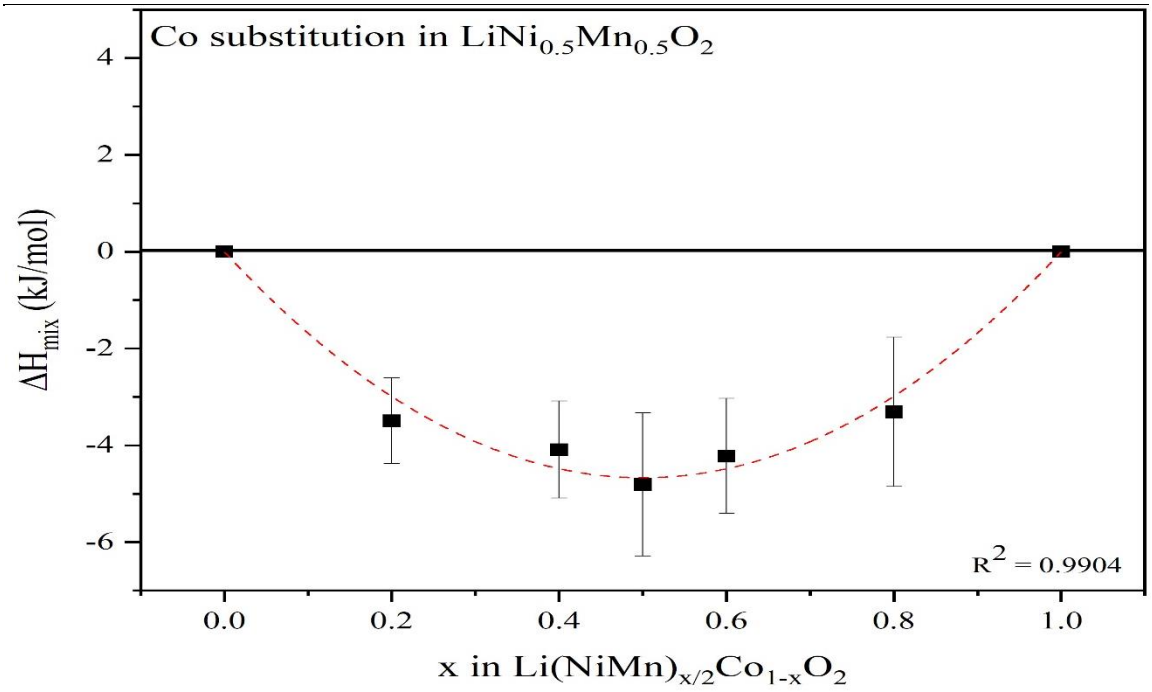

Figure 7 Enthalpy of Mixing of the Cobalt Solid Solution Series

Figure 7 shows that NMC2.5,2.5,5 has the most exothermic heat of mixing which means it is more stable relative to the end members than the other compositions in the cobalt series. In terms of greatest to least heats of mixing the NMCs were: NMC334, NMC226, NMC118, and NMC442. The two end members have heat of mixing of zero (by definition).

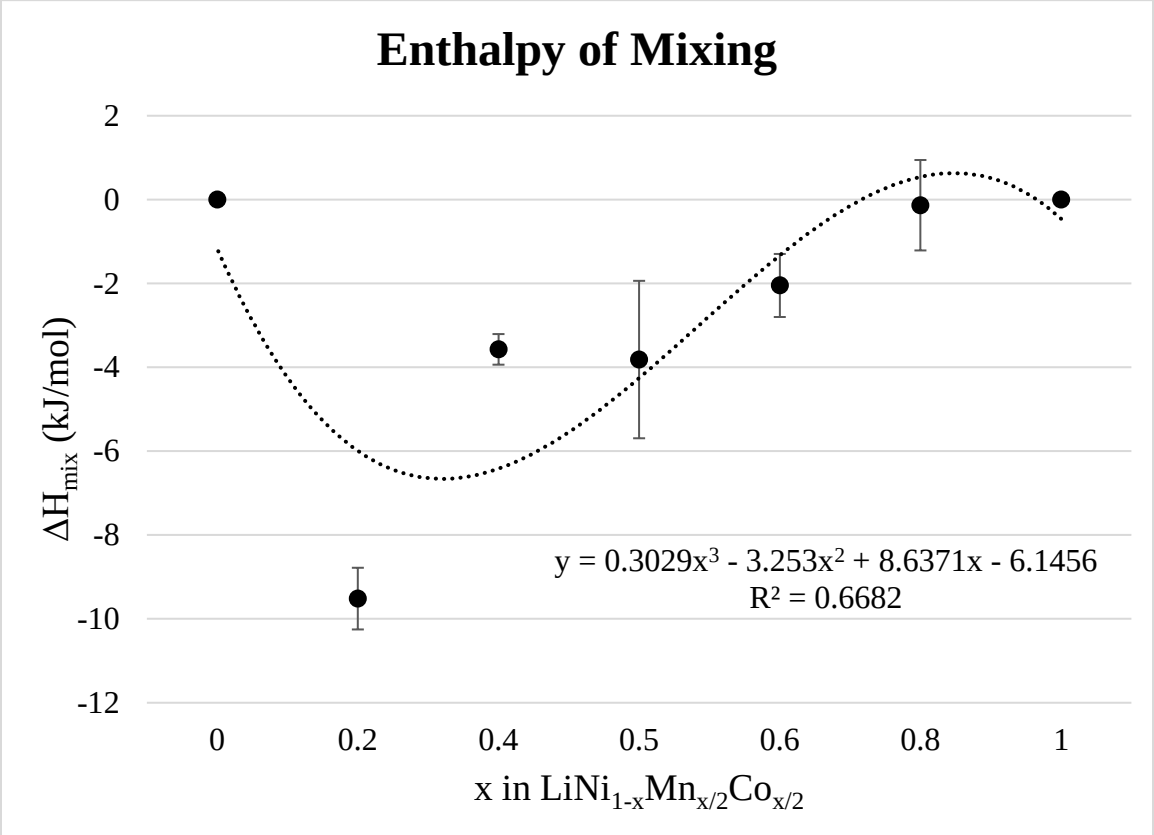

Figure 8 Enthalpy of Mixing of the Nickel Solid Solution Series

Figure 8 shows the enthalpies of mixing for the nickel solid solution series. This series is not a regular solution and can be fit with a third order polynomial. NMC811 has the most exothermic heat of mixing with a value of -9.516±0.74 kJ/mol meaning it is

most stable relative to the end members for this series. The enthalpy of formation for NMC811 is much larger in magnitude than any other solid solution samples in this series and may need to be remeasured. The remaining NMCs have negative enthalpies of mixing. NMC244 had a heat of mixing that was nearly positive which would mean it is not thermodynamically stable at room temperature.

Table 6

Enthalpies of Drop Solution at 800 °C, Enthalpies of Formation at 25 °C, and Enthalpies of Mixing at 25 °C

Sample	H_{DS} (kJ/mol)	H_{FE} (kJ/mol)	H_{mix} (kJ/mol)
$LiCo_{0.5}Mn_{0.5}O_2$	145.39±0.63 (n)	-126.741±1.80	0±0
$LiNi_{0.2}Mn_{0.4}Co_{0.4}O_2$	129.41±0.95	-112.61±1.92	-0.134±1.08
$LiNi_{0.4}Mn_{0.3}Co_{0.3}O_2$	115.21±0.63	-100.26±1.85	-2.048±0.75
$LiNi_{0.5}Mn_{0.25}Co_{0.25}O_2$	108.92±1.84	-94.89±2.48	-3.815±1.88
$LiNi_{0.6}Mn_{0.2}Co_{0.2}O_2$	100.62±0.11	-87.51±1.67	-3.572±0.36
$LiNi_{0.8}Mn_{0.1}Co_{0.1}O_2$	90.45±0.65	-79.19±1.79	-9.516±0.74
$LiNiO_2$	64.82±0.4	-76.26±1.72	0±0

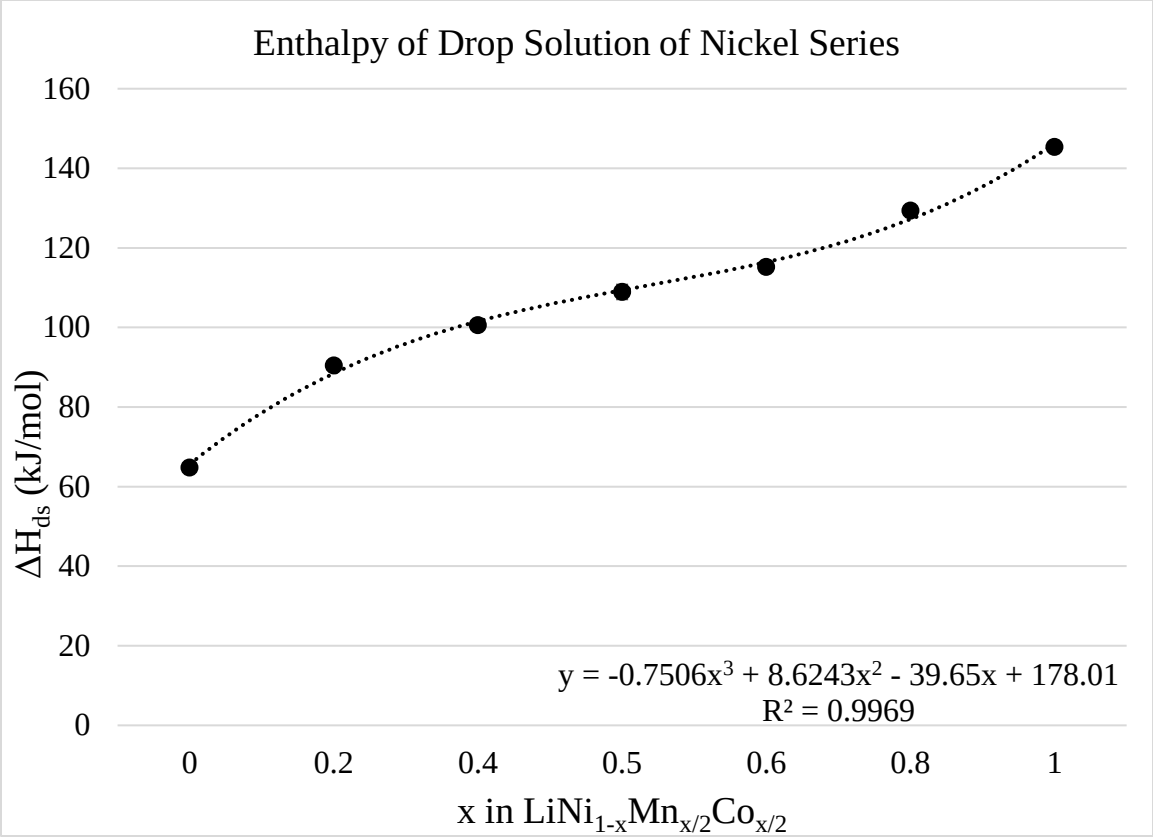

Figure 9 Enthalpy of Drop Solution of the Nickel Series

As seen in Table 6 and Figure 9, the heats of drop solution had the greatest value of 145.39±0.63 kJ/mol in $LiCo_{0.5}Mn_{0.5}O_2$ and a low of 64.82±0.4 kJ/mol in $LiNiO_2$. The enthalpy of formation ranged from -126.741±1.80 kJ/mol for $LiCo_{0.5}Mn_{0.5}O_2$ to -76.258±1.72 kJ/mol for $LiCoO_2$ in the nickel series.

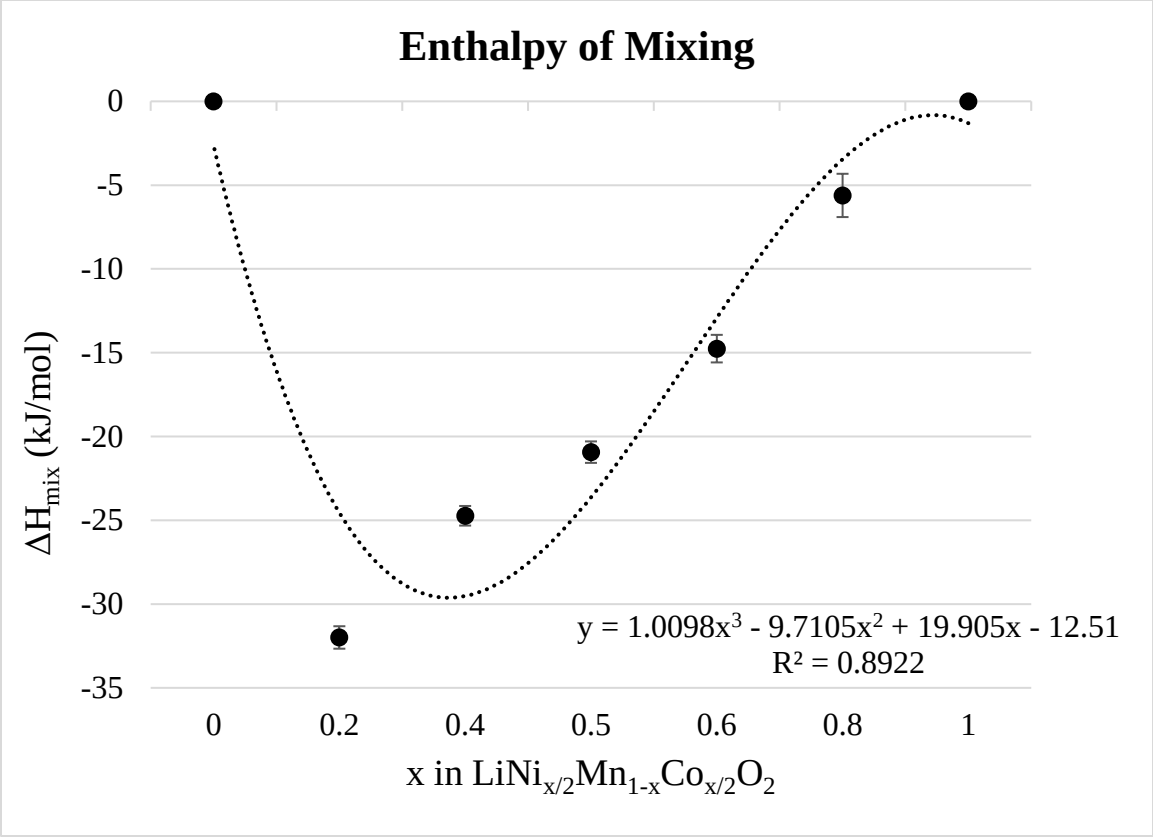

Figure 10 Enthalpy of Mixing of the Manganese Solid Solution Series

Figure 10 shows the enthalpy of mixing of the manganese solid solution series. In relation to the end members of the series, Li_2MnO_3 and $LiNi_{0.5}Co_{0.5}O_2$, NMC181 displayed the most stable energetics as it had the most negative value of -31.99 ±0.67 kJ/mol. All the solid solutions in this series had negative heats of mixing and could be fit with a third order polynomial. The trend is similar to the nickel series. In terms of stability, the most to the least stable is: NMC181, NMC262, NMC2.5,5,2.5, NMC343, and NMC424. This means for the solid solutions that as the amount of manganese is decreased, the stability of the NMC also decreases.

Table 7 shows the heats of drop solution, formation and mixing for the manganese series.

Table 7

Enthalpies of Drop Solution at 800 °C, Enthalpies of Formation at 25 °C, and Enthalpies of Mixing at 25 °C

Sample	H_{DS} (kJ/mol)	H_{FE} (kJ/mol)	H_{mix} (kJ/mol)
$LiNi_{0.5}Co_{0.5}O_2$	94.62±0.97 (n)	-98.53±1.92	0±0
$LiNi_{0.4}Mn_{0.2}Co_{0.4}O_2$	107.16±1.03	-99.38±1.97	-5.61±1.29
$LiNi_{0.3}Mn_{0.4}Co_{0.3}O_2$	123.23±0.56	-103.76±1.76	-14.76±0.82
$LiNi_{0.25}Mn_{0.5}Co_{0.25}O_2$	132.87±0.37	-107.56±1.72	-20.93±0.64
$LiNi_{0.2}Mn_{0.6}Co_{0.2}O_2$	140.13±0.37	-108.97±1.73	-24.73±0.58
$LiNi_{0.1}Mn_{0.8}Co_{0.1}O_2$	154.32±0.56	-111.47±1.82	-31.99±0.67
Li_2MnO_3	129.25±0.39	-108.07±3.37	0±0

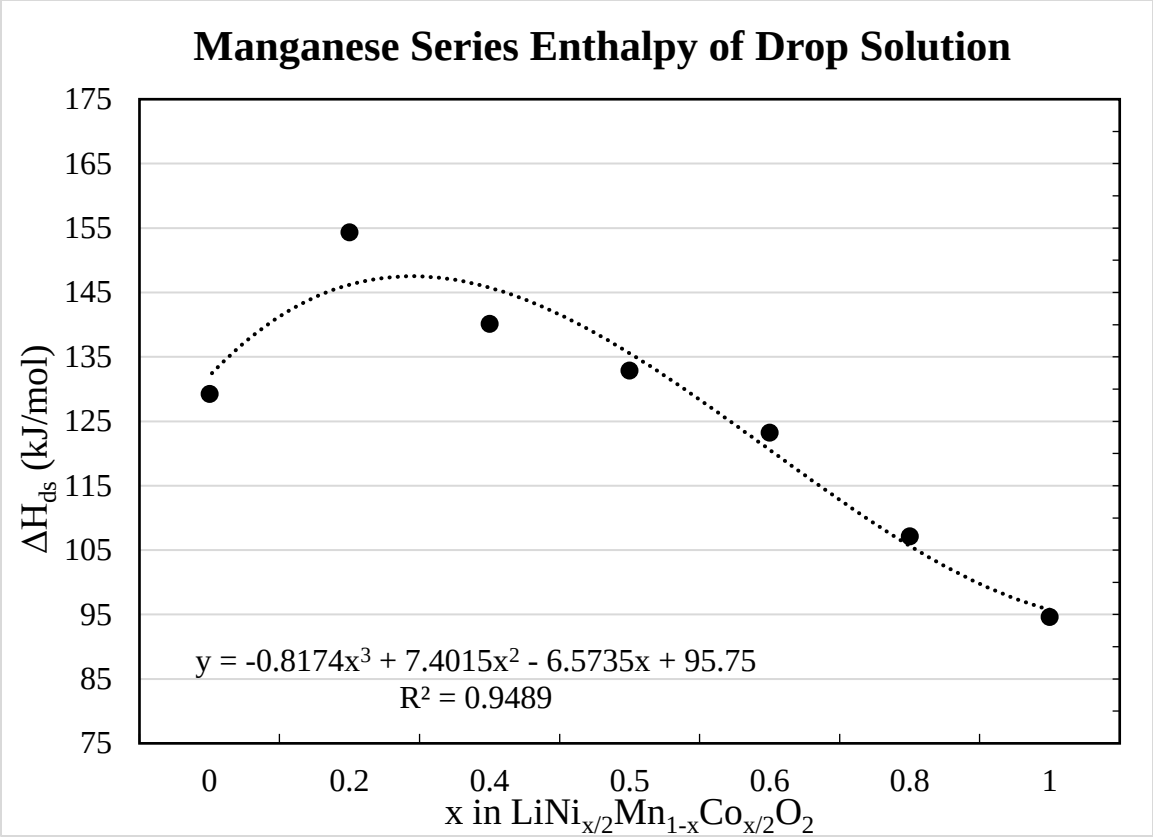

Figure 11 Enthalpy of Drop Solution of the Manganese Series

Figure 11 shows the enthalpy of drop solution of the manganese series. NMC181 had the highest heat of drop solution and also had the most negative formation and mixing enthalpy. The other solid solutions fell in order of decreasing formation enthalpy and drop solution enthalpy based upon decreasing manganese concentration. The end member Li_2MnO_3 did not follow the trend of the series possibly due to its different structure.

CHAPTER 4

CONCLUSIONS

The NMC cathode materials were successfully synthesized by a sol-gel method. The lattice parameters of various molar ratios of NMC materials were determined by powder X-ray diffraction. The lattice parameters of the cobalt ($LiNi_{x/2}Mn_{x/2}Co_{1-x}$) and nickel solid solution ($LiNi_{1-x}Mn_{x/2}Co_{x/2}O_2$) follow approximately linear trends, with lattice parameters increasing for Co and decreasing for Ni substitution. The manganese series did not follow a linear trend but in general the lattice constant decreased with decreasing Mn concentration. The enthalpies of drop solution of these series in molten sodium molybdate solvent at 800 °C were measured. The enthalpies of mixing, calculated from these data, are generally exothermic and are being analyzed further.

REFERENCES

1. Driscoll, E. H., et al. “The Building Blocks of Battery Technology: Using Modified Tower Block Game Sets to Explain and Aid the Understanding of Rechargeable Li-Ion Batteries.” *Journal of Chemical Education*, vol. 97, no. 8, 2020, pp. 2231–2237., https://doi.org/10.1021/acs.jchemed.0c00282.

2. Zaghib, Karim, et al. “Advanced Electrodes for High Power Li-Ion Batteries.” *Materials*, vol. 6, no. 3, 2013, pp. 1028–1049., https://doi.org/10.3390/ma6031028.

3. Li, Wangda, et al. “High-Nickel Layered Oxide Cathodes for Lithium-Based Automotive Batteries.” *Nature Energy*, vol. 5, no. 1, 2020, pp. 26–34., https://doi.org/10.1038/s41560-019-0513-0

4. Summerfield, John. “Modeling the Lithium Ion Battery.” *Journal of Chemical Education*, vol. 90, no. 4, 2013, pp. 453–455., https://doi.org/10.1021/ed300533f.

5. Wang, M. “Enthalpy of Formation of LiNiO2, licoo2 and Their Solid Solution, lini1−xcoxo2.” *Solid State Ionics*, vol. 166, no. 1-2, 2004, pp. 167–173., https://doi.org/10.1016/j.ssi.2003.11.004.

6. Mansour, Seham A.A. “Spectrothermal Studies on the Decomposition Course of Cobalt Oxysalts Part II. Cobalt Nitrate Hexahydrate.” *Materials Chemistry and Physics*, vol. 36, no. 3-4, 1994, pp. 317–323., https://doi.org/10.1016/0254-0584(94)90048-5.

7. Gallagher, P.K., et al. “The Thermal Decomposition of Aqueous Manganese (II) Nitrate Solution.” *Thermochimica Acta*, vol. 2, no. 5, 1971, pp. 405–412., https://doi.org/10.1016/0040-6031(71)85016-5.

8. Zhao, Hong, et al. “Cobalt-Free Cathode Materials: Families and Their Prospects.” *Advanced Energy Materials*, vol. 12, no. 16, 2022, p. 2103894., https://doi.org/10.1002/aenm.202103894.

9. Coppo, Paolo. “Lithium Ion Battery Cathode Materials as a Case Study to Support the Teaching of Ionic Solids.” *Journal of Chemical Education*, vol. 94, no. 8, 2017, pp. 1174–1178., https://doi.org/10.1021/acs.jchemed.6b00569.

10. Goodenough, John B. “How We Made the Li-Ion Rechargeable Battery.” *Nature Electronics*, vol. 1, no. 3, 2018, pp. 204–204., https://doi.org/10.1038/s41928-018-0048-6.

11. Maharaj, Franklin D., et al. “Exploring Real-World Applications of Electrochemistry by Constructing a Rechargeable Lithium-Ion Battery.” *Journal of Chemical Education*, vol. 96, no. 12, 2019, pp. 3014–3017., https://doi.org/10.1021/acs.jchemed.9b00328.

12. Navrotsky, Alexandra. “Progress and New Directions in High Temperature Calorimetry Revisited.” *Physics and Chemistry of Minerals*, vol. 24, no. 3, 1997, pp. 222–241., https://doi.org/10.1007/s002690050035.

13. Navrotsky, Alexandra. “Progress and New Directions in High Temperature Calorimetry.” *Physics and Chemistry of Minerals*, vol. 2, no. 1-2, 1977, pp. 89–104., https://doi.org/10.1007/bf00307526.

14. Toby, B. H., & Von Dreele, R. B. (2013). "GSAS-II: the genesis of a modern open-source all purpose crystallography software package". *Journal of Applied Crystallography*, **46**(2), 544-549. doi:10.1107/S0021889813003531

15. Shannon, R. D. “Revised Effective Ionic Radii and Systematic Studies of Interatomic Distances in Halides and Chalcogenides.” *Acta Crystallographica Section A*, vol. 32, no. 5, 1976, pp. 751–767., https://doi.org/10.1107/s0567739476001551.

16. Subramani, Tamilarasan, and Alexandra Navrotsky. “Thermochemistry of Cation Disordered Li Ion Battery Cathode Materials, (M′ = Nb and Ta, M″ = Mn and Fe).” *RSC Advances*, vol. 10, no. 11, 2020, pp. 6540–6546., https://doi.org/10.1039/c9ra09759g.

17. Hayun, S., et al. “Enthalpies of Formation of High Entropy and Multicomponent Alloys Using Oxide Melt Solution Calorimetry.” *Intermetallics*, vol. 125, 2020, p. 106897., https://doi.org/10.1016/j.intermet.2020.106897.

18. R.A. Robie, B.S. Hemingway, Thermodynamic Properties of Minerals and Related Substances at 298.15 K and 1 bar (105 Pascals) Pressure and at Higher Temperatures, U.S. Geological Survey Bulletin 2131, Washington, DC, 1995.

19. Ehrhardt, Claus, et al. “Thermal Decomposition of Cobalt Nitrato Compounds: Preparation of Anhydrous Cobalt(Ii)Nitrate and Its Characterisation by Infrared and Raman Spectra.” *Thermochimica Acta*, vol. 432, no. 1, 2005, pp. 36–40., https://doi.org/10.1016/j.tca.2005.04.010.

20. Garche, Jürgen, and Klaus Brandt. *Electrochemical Power Sources: Fundamentals, Systems, and Applications: Li-Battery Safety*. Elsevier, 2019.

APPENDIX A

SERIES UNIT CELL PARAMETERS *A* AND *C*

Cobalt Unit Cell Parameters:

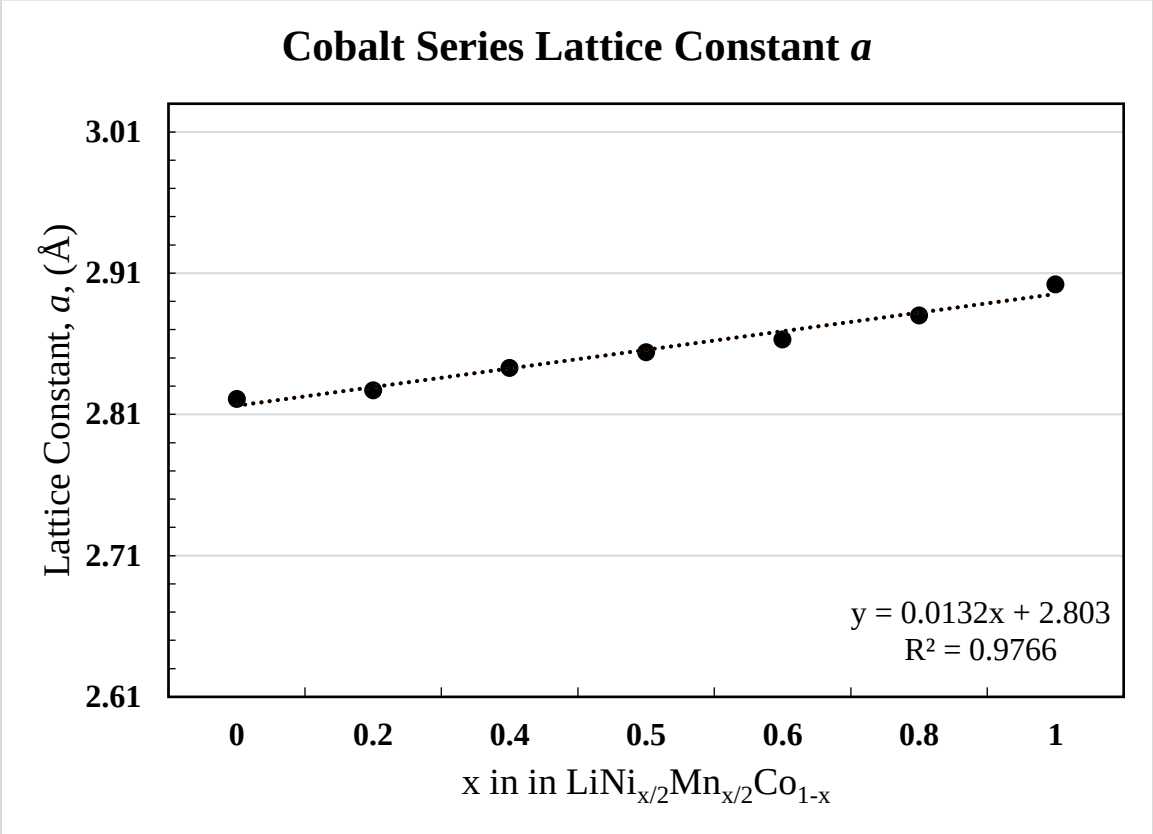

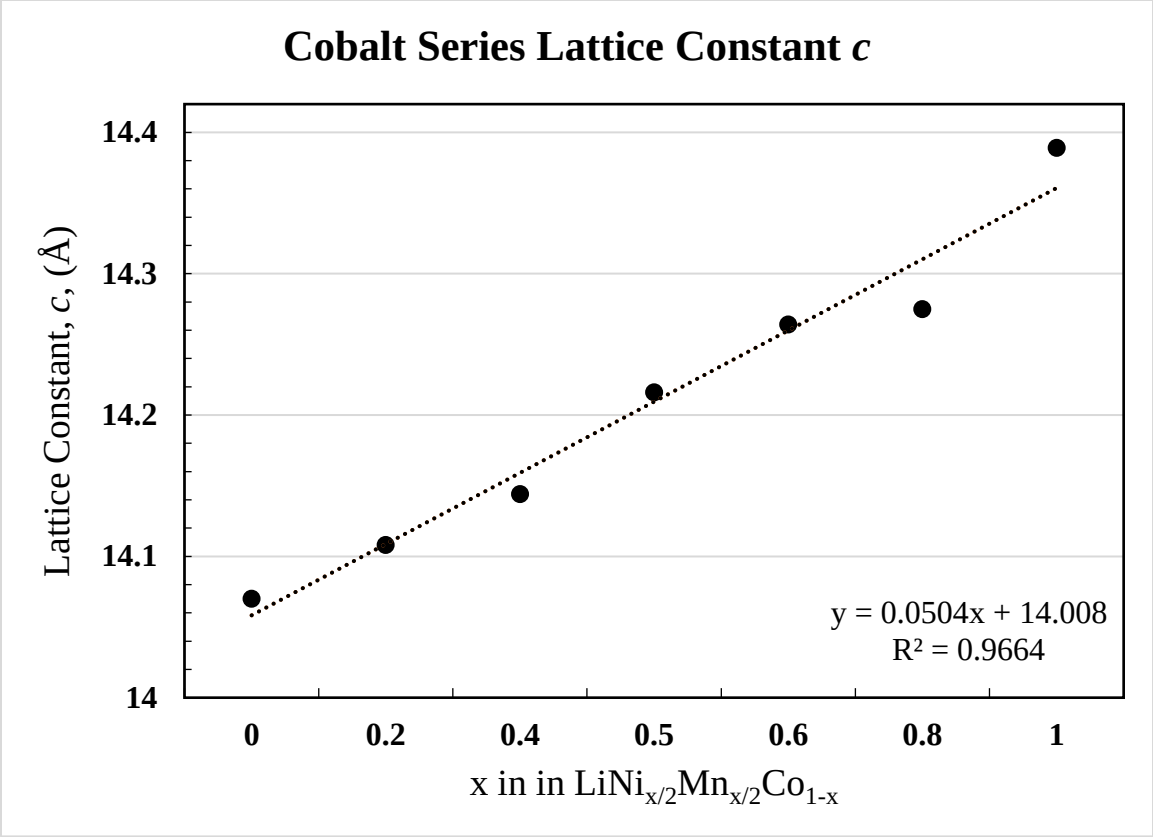
Cobalt Series Lattice Constant c
Lattice Constant, c, (Å)
14.4
14.3
14.2
14.1
14
0
0.2
0.4
0.5
0.6
0.8
1
x in in LiNi$_{x/2}$Mn$_{x/2}$Co$_{1-x}$
y = 0.0504x + 14.008
R² = 0.9664

Nickel Unit Cell Parameters:

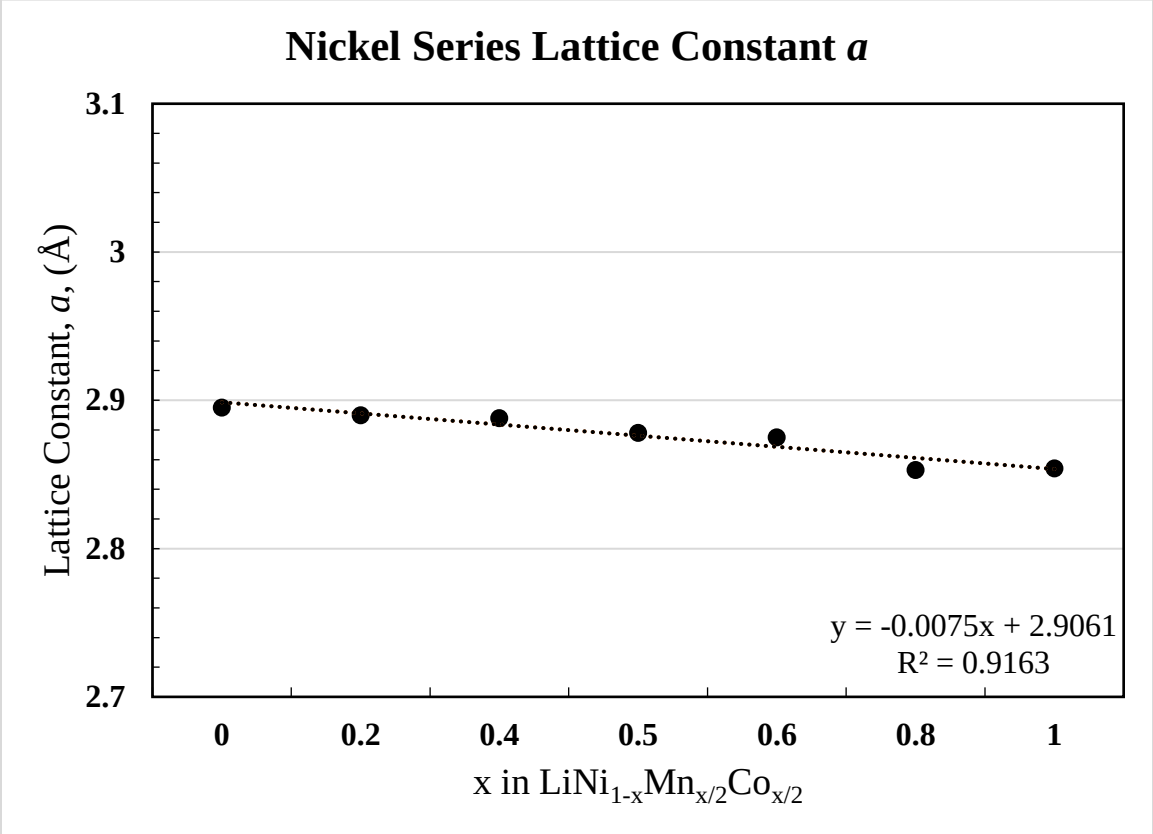

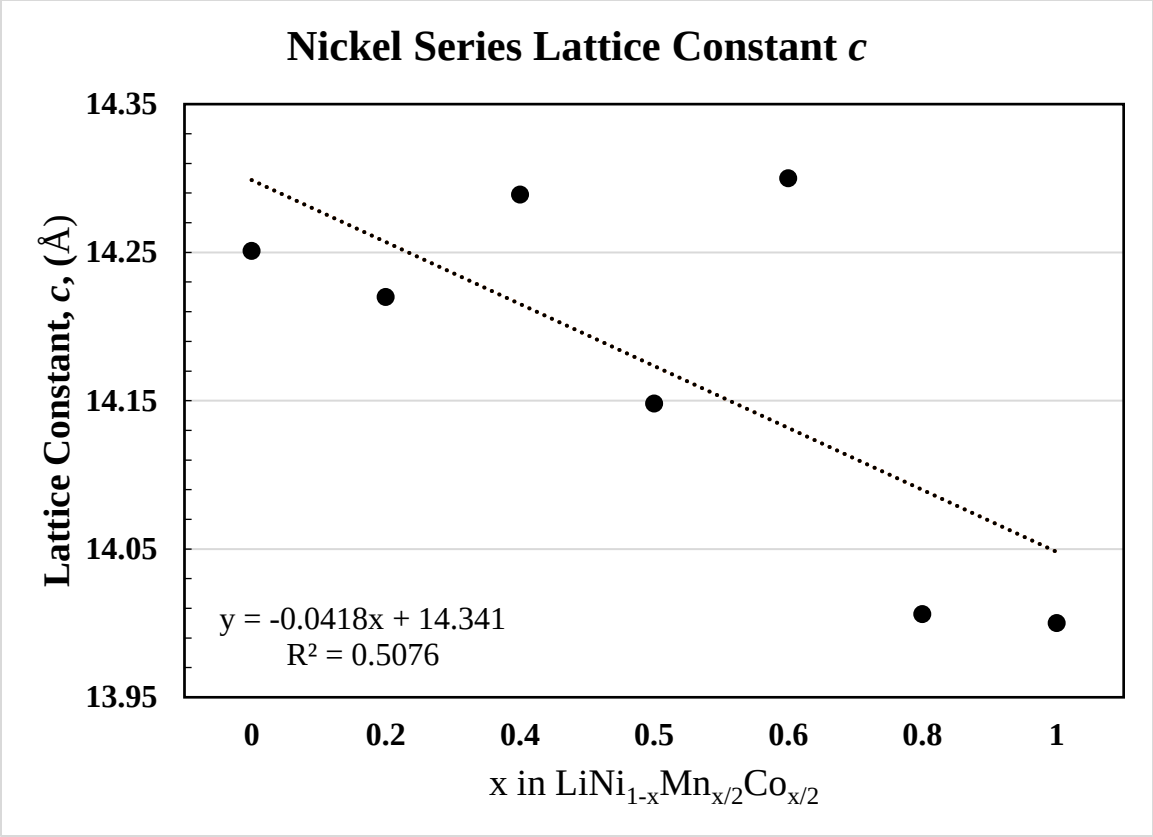
Nickel Series Lattice Constant c
Lattice Constant, c, (Å)
14.35
14.25
14.15
14.05
13.95
y = -0.0418x + 14.341
R² = 0.5076
0
0.2
0.4
0.5
0.6
0.8
1
x in LiNi1-xMnx/2Cox/2

Manganese Unit Cell Parameters:

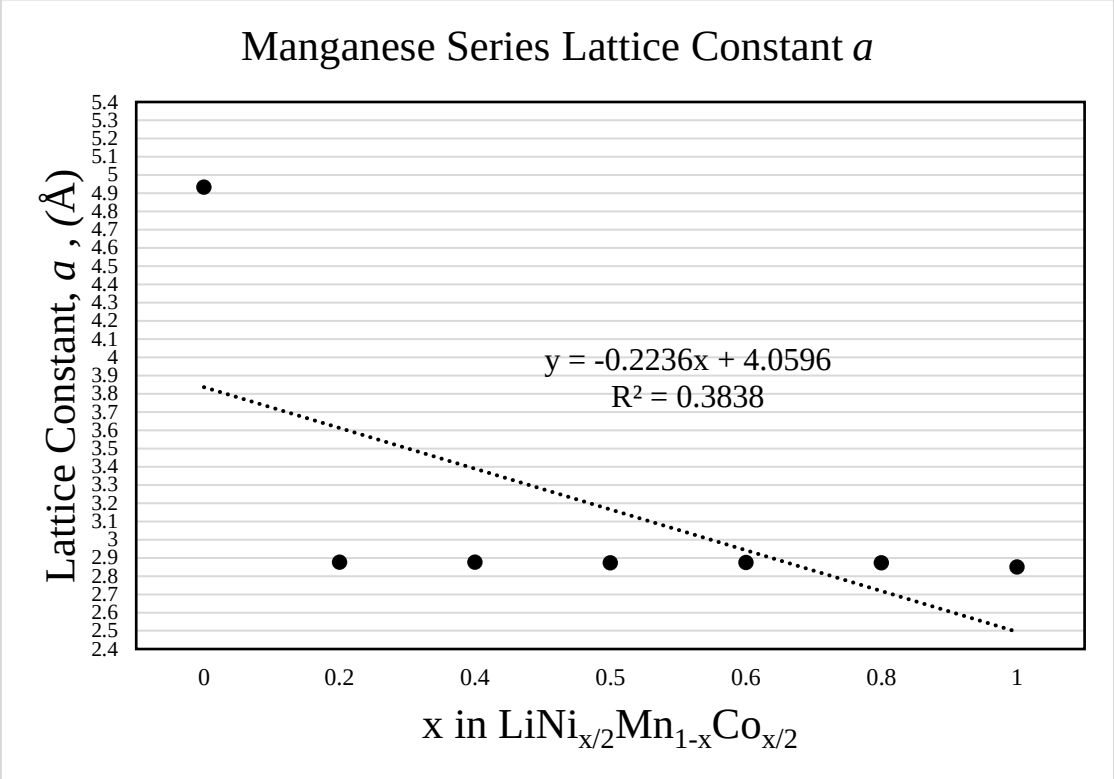

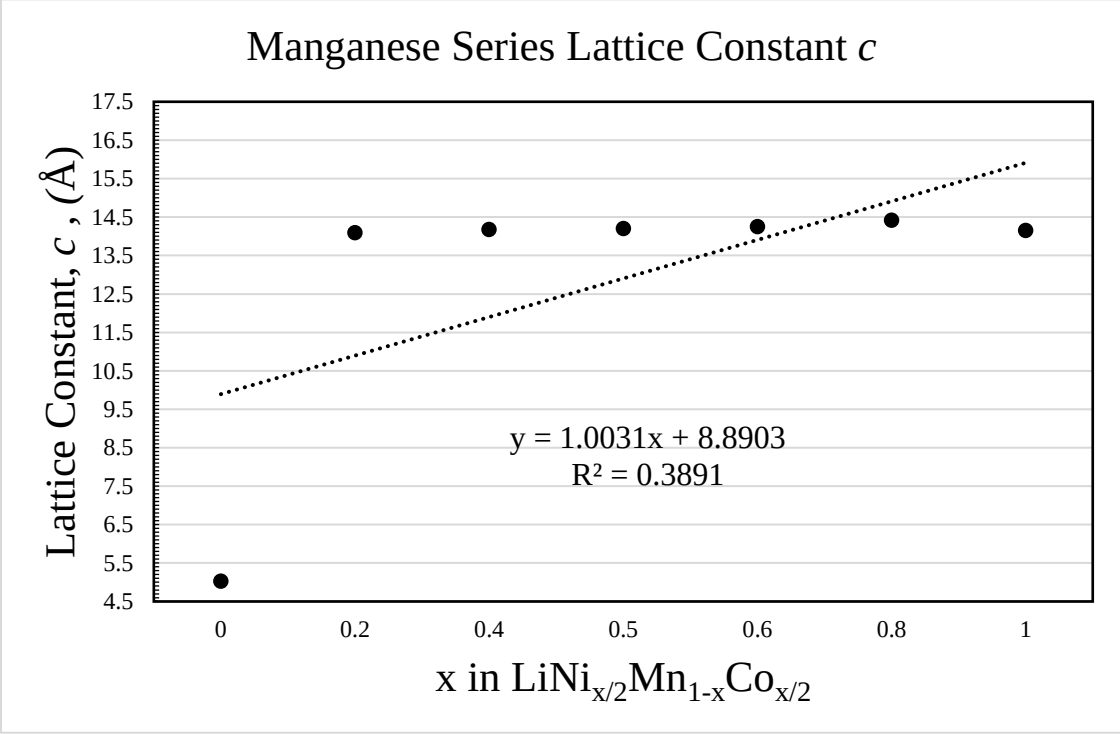

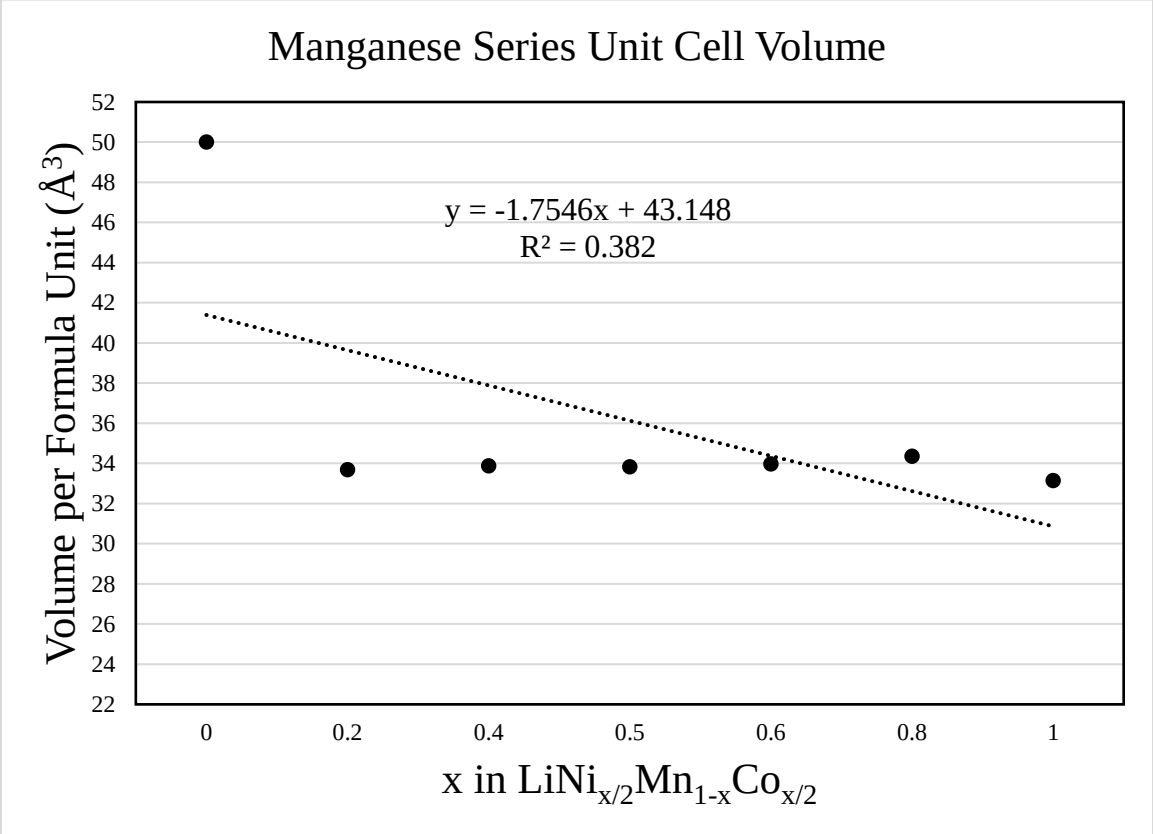
Manganese Series Unit Cell Volume
Volume per Formula Unit (Å3)
52
50
48
46
44
42
40
38
36
34
32
30
28
26
24
22
y = -1.7546x + 43.148
R² = 0.382
0
0.2
0.4
0.5
0.6
0.8
1
x in LiNix/2Mn1-xCox/2

APPENDIX B

XRD PATTERNS

XRD Patterns:

Cobalt Series (in descending cobalt content):

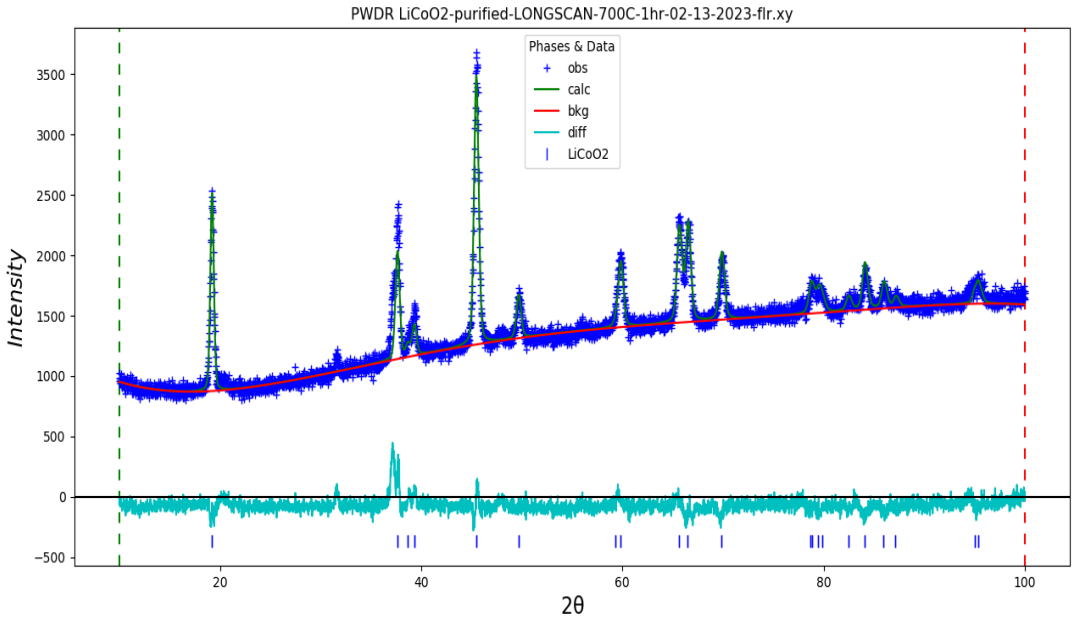

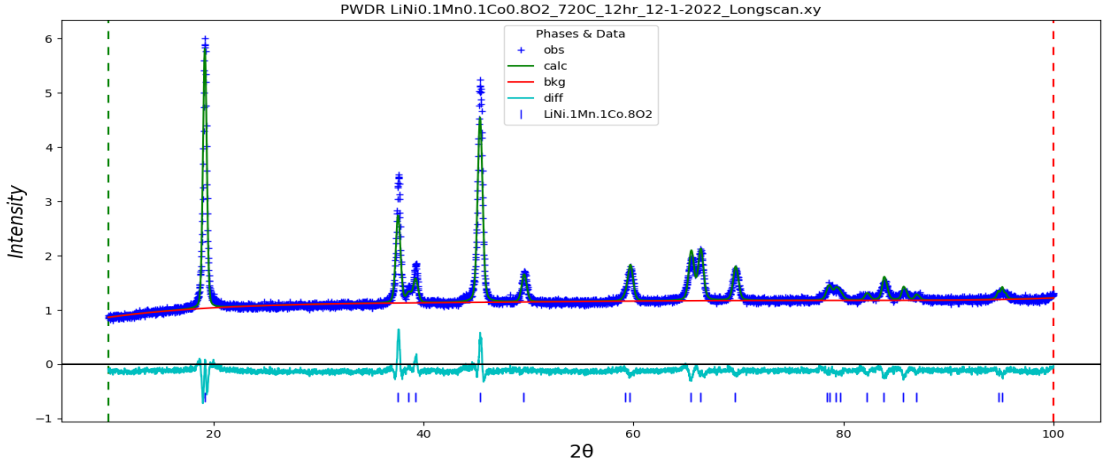
PWDR LiNi0.1Mn0.1Co0.8O2_720C_12hr_12-1-2022_Longscan.xy
Phases & Data
obs
calc
bkg
diff
LiNi.1Mn.1Co.8O2
Intensity
2θ

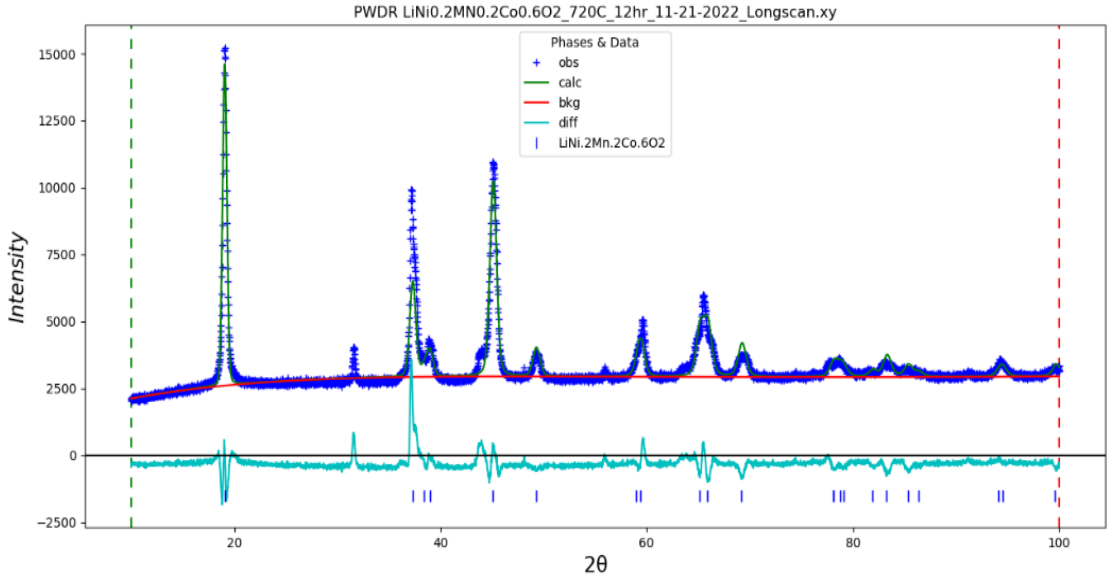
PWDR LiNi0.2MN0.2Co0.6O2_720C_12hr_11-21-2022_Longscan.xy
Phases & Data
obs
calc
bkg
diff
LiNi.2Mn.2Co.6O2
Intensity
2θ

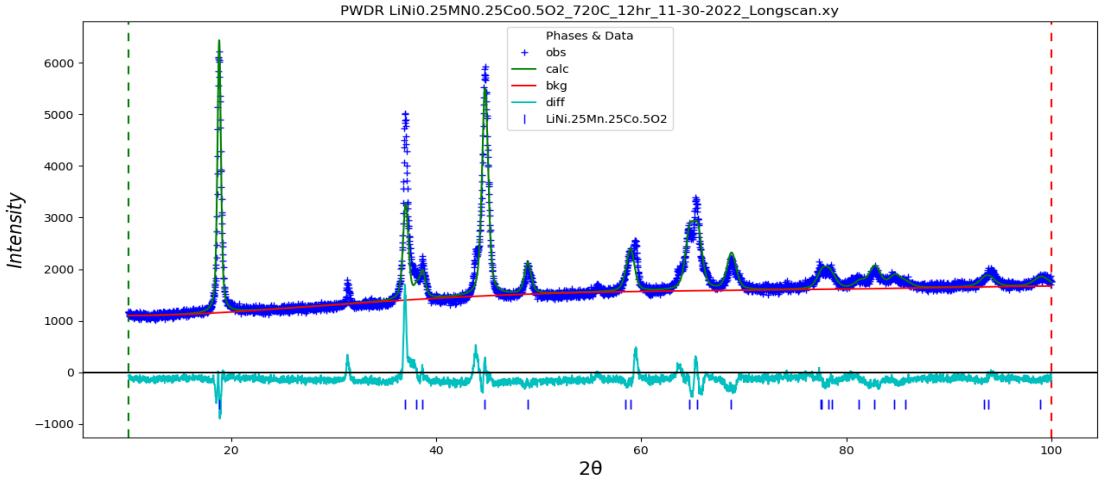
PWDR LiNi0.25MN0.25Co0.5O2_720C_12hr_11-30-2022_Longscan.xy
Phases & Data
obs
calc
bkg
diff
LiNi.25Mn.25Co.5O2
Intensity
2θ

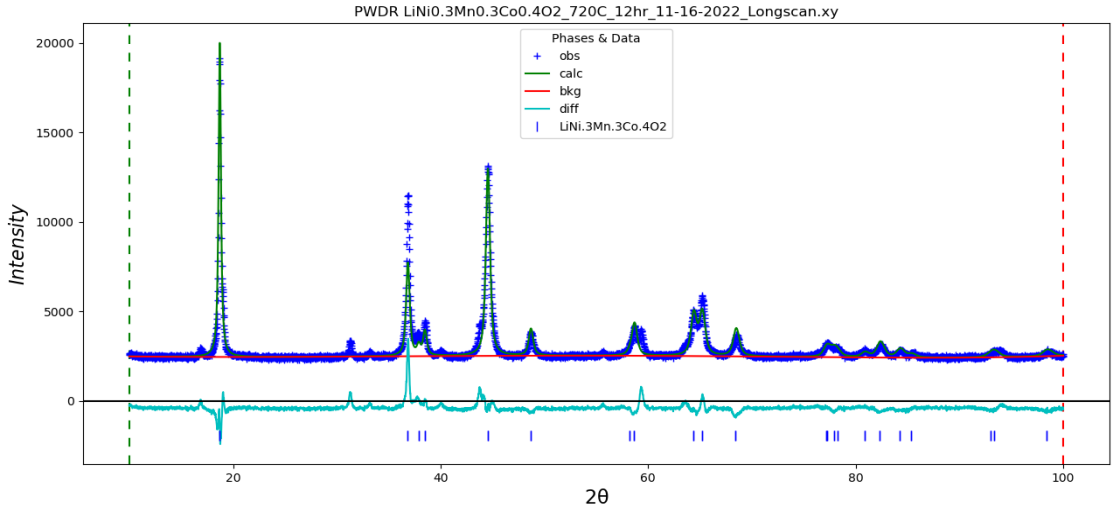
PWDR LiNi0.3Mn0.3Co0.4O2_720C_12hr_11-16-2022_Longscan.xy
Phases & Data
obs
calc
bkg
diff
LiNi.3Mn.3Co.4O2
Intensity
2θ

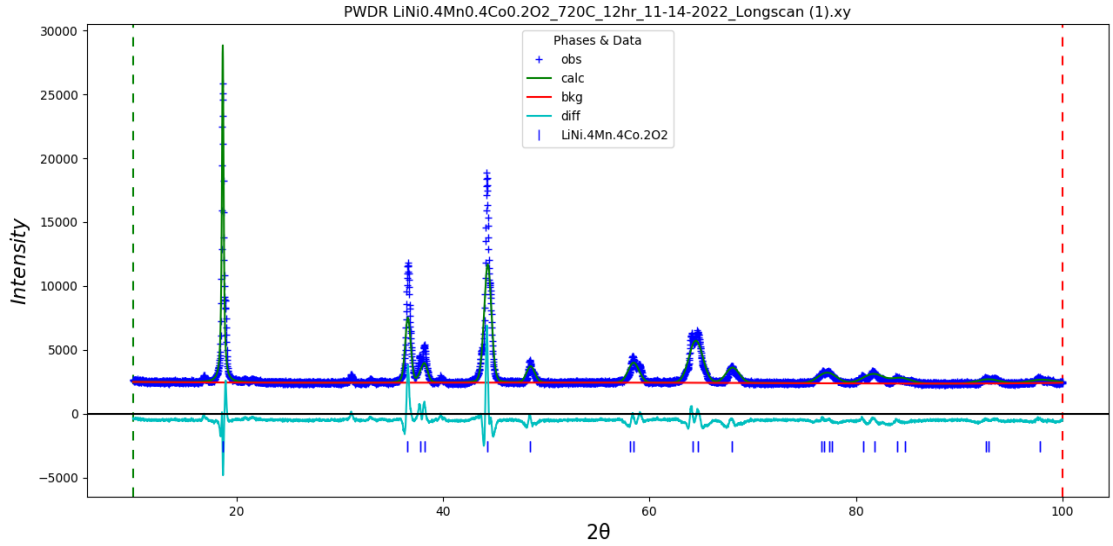
PWDR LiNi0.4Mn0.4Co0.2O2_720C_12hr_11-14-2022_Longscan (1).xy
Phases & Data
obs
calc
bkg
diff
LiNi.4Mn.4Co.2O2
Intensity
2θ

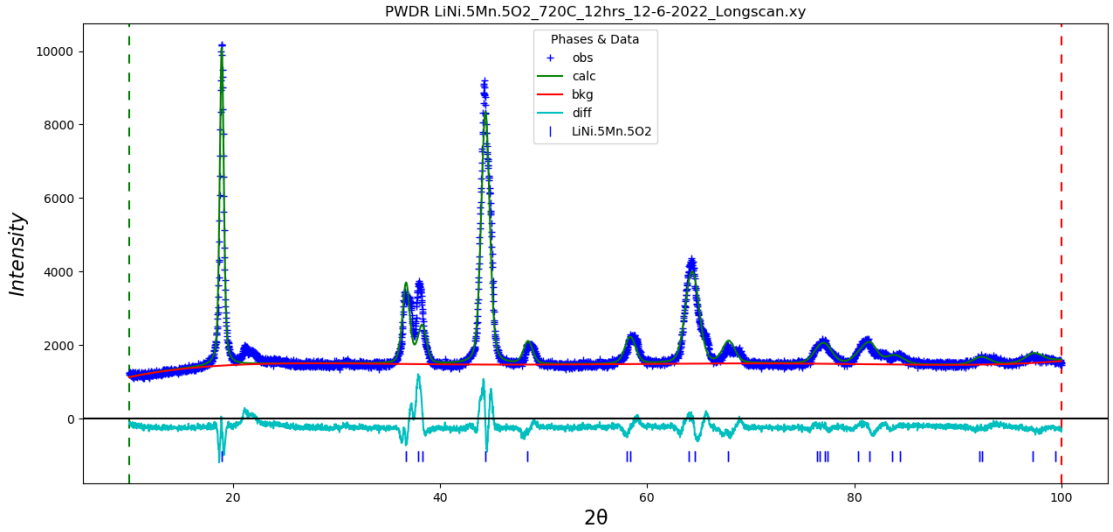
PWDR LiNi.5Mn.5O2_720C_12hrs_12-6-2022_Longscan.xy
Phases & Data
obs
calc
bkg
diff
LiNi.5Mn.5O2
Intensity
2θ

Nickel Series (in descending nickel content):

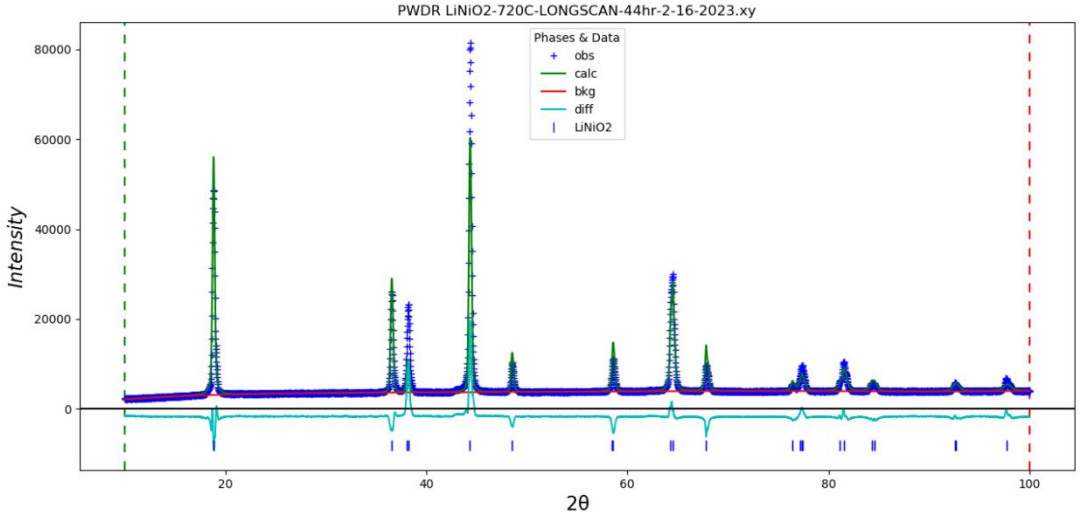

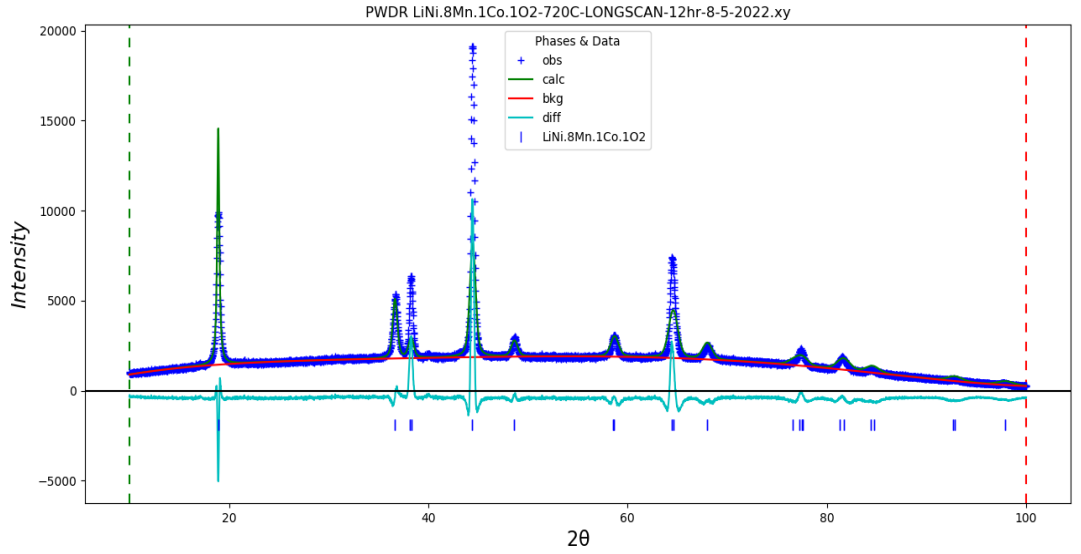

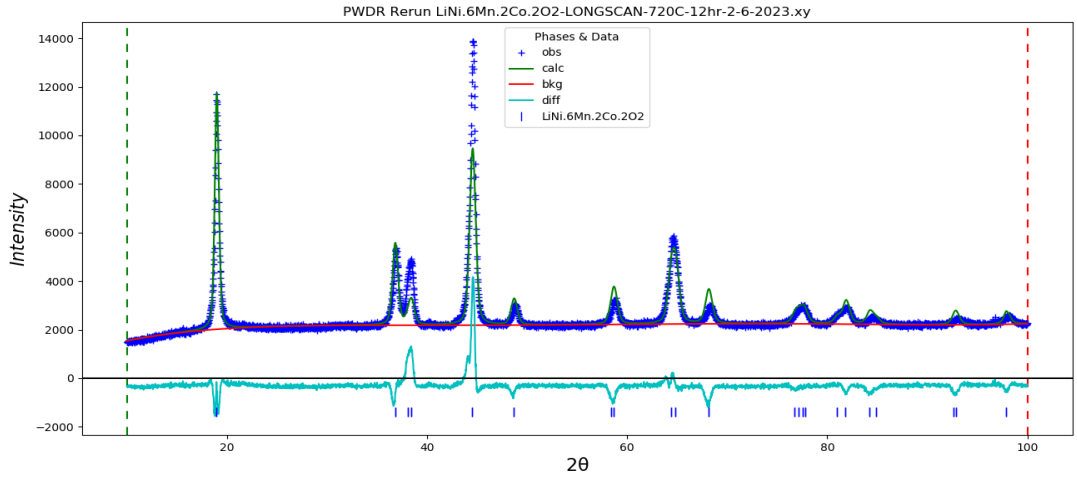

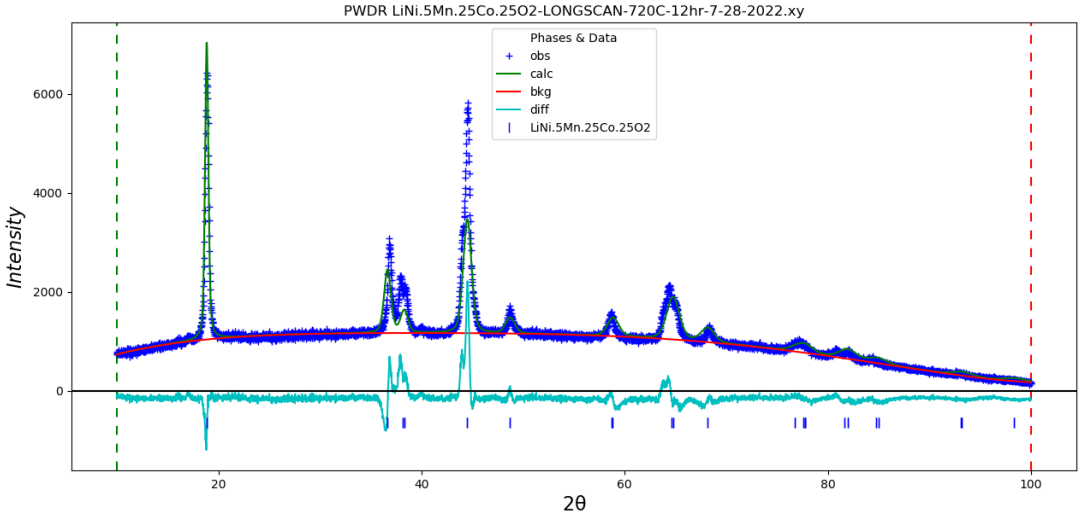
PWDR LiNi.5Mn.25Co.25O2-LONGSCAN-720C-12hr-7-28-2022.xy
Phases & Data
obs
calc
bkg
diff
LiNi.5Mn.25Co.25O2
Intensity
2θ

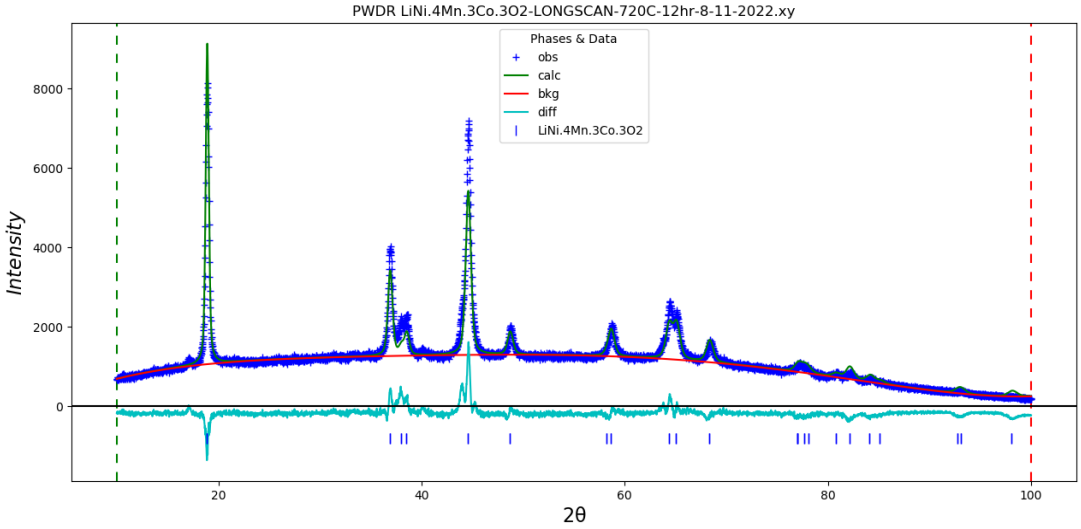
PWDR LiNi.4Mn.3Co.3O2-LONGSCAN-720C-12hr-8-11-2022.xy
Phases & Data
obs
calc
bkg
diff
LiNi.4Mn.3Co.3O2
Intensity
2θ

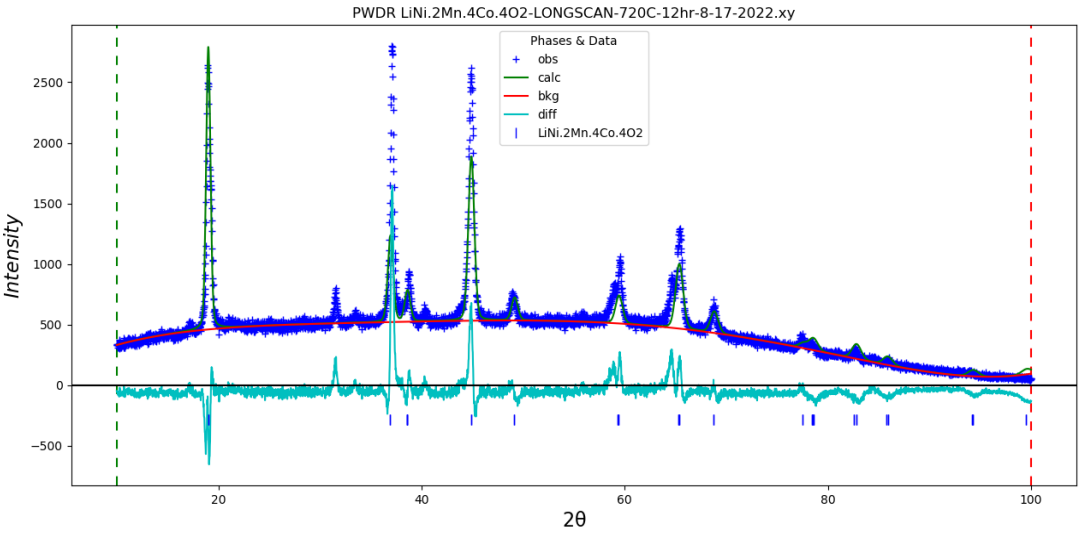
PWDR LiNi.2Mn.4Co.4O2-LONGSCAN-720C-12hr-8-17-2022.xy
Phases & Data
obs
calc
bkg
diff
LiNi.2Mn.4Co.4O2
Intensity
2θ

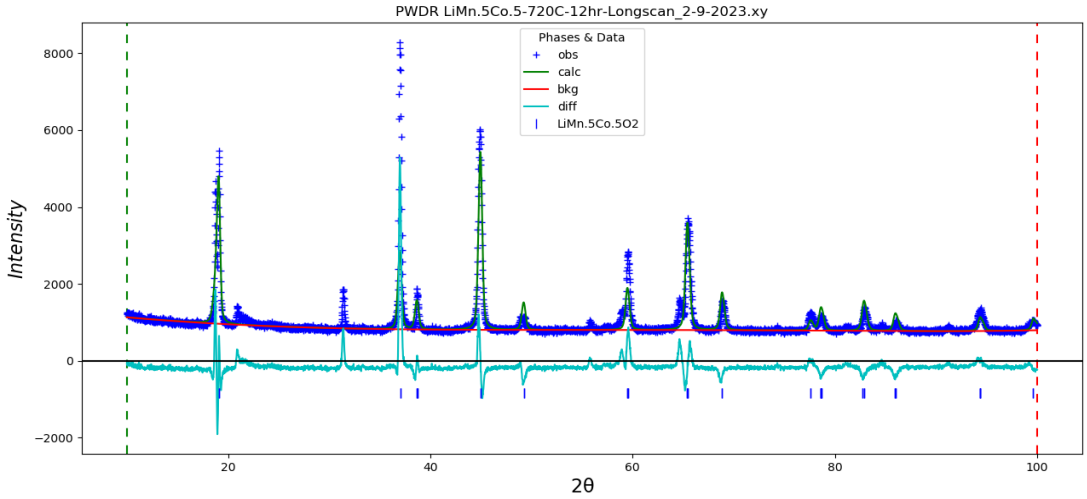

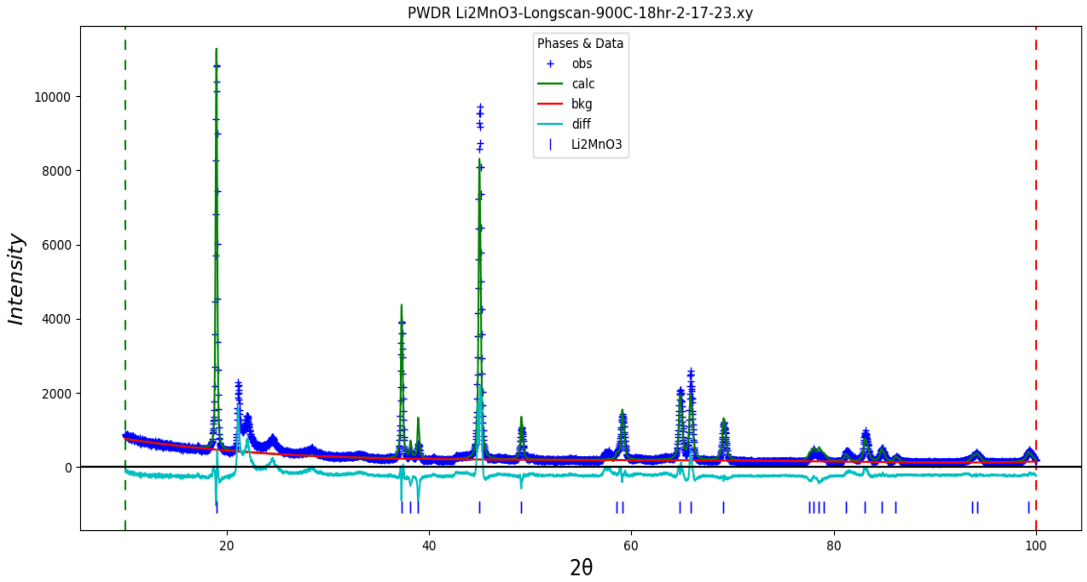

Manganese Series (in descending manganese content):

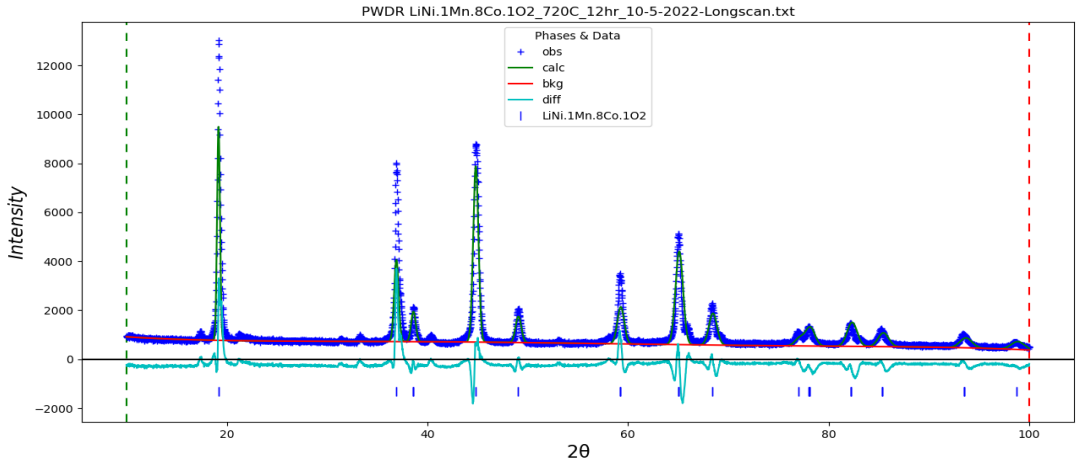
PWDR LiNi.1Mn.8Co.1O2_720C_12hr_10-5-2022-Longscan.txt
Phases & Data
obs
calc
bkg
diff
LiNi.1Mn.8Co.1O2
Intensity
2θ

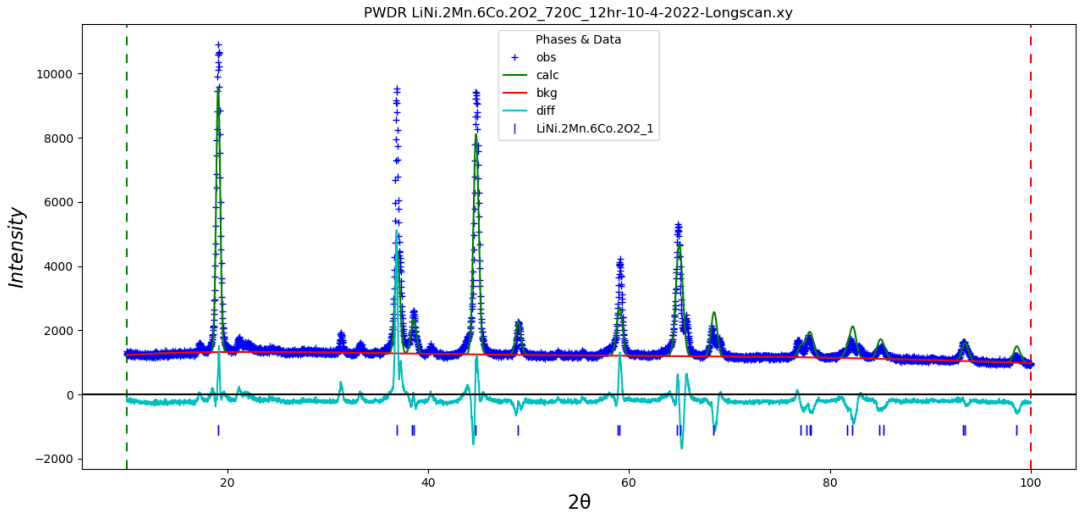
PWDR LiNi.2Mn.6Co.2O2_720C_12hr-10-4-2022-Longscan.xy
Phases & Data
obs
calc
bkg
diff
LiNi.2Mn.6Co.2O2_1
Intensity
2θ

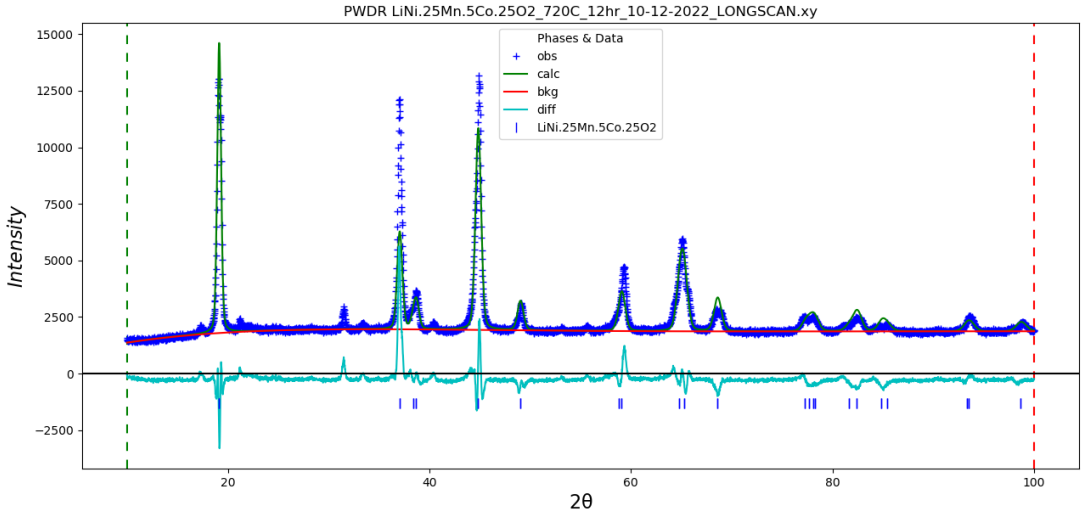
PWDR LiNi.25Mn.5Co.25O2_720C_12hr_10-12-2022_LONGSCAN.xy
Phases & Data
obs
calc
bkg
diff
LiNi.25Mn.5Co.25O2
Intensity
2θ

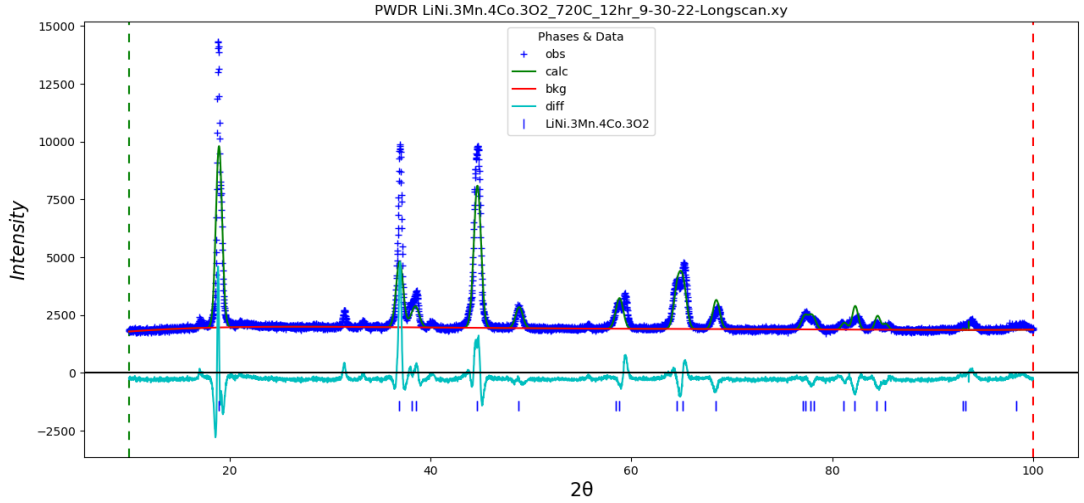
PWDR LiNi.3Mn.4Co.3O2_720C_12hr_9-30-22-Longscan.xy
Phases & Data
obs
calc
bkg
diff
LiNi.3Mn.4Co.3O2
Intensity
2θ

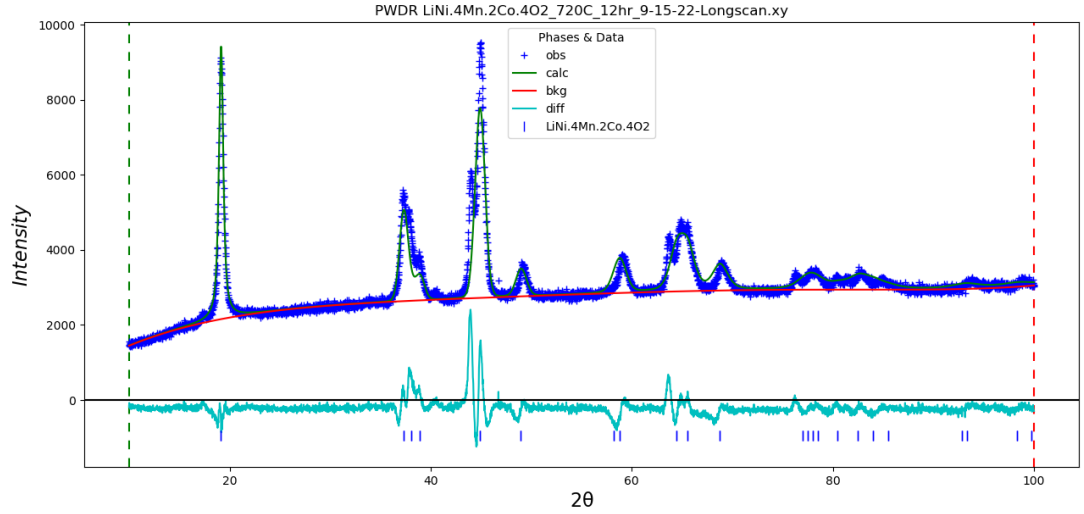
PWDR LiNi.4Mn.2Co.4O2_720C_12hr_9-15-22-Longscan.xy
Phases & Data
obs
calc
bkg
diff
LiNi.4Mn.2Co.4O2
Intensity
2θ

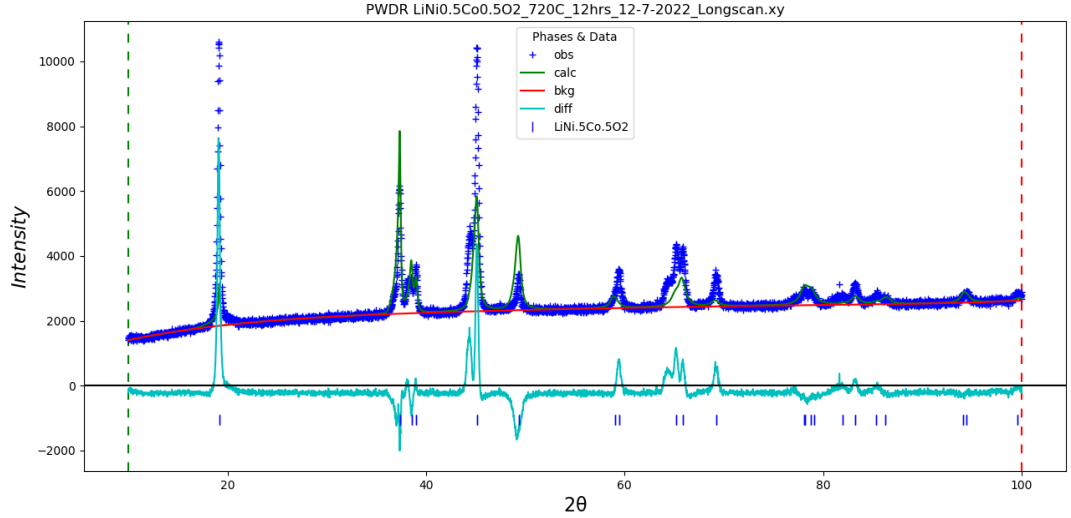
PWDR LiNi0.5Co0.5O2_720C_12hrs_12-7-2022_Longscan.xy
Phases & Data
obs
calc
bkg
diff
LiNi.5Co.5O2
Intensity
2θ

APPENDIX C

CALORIMETRY DATA

Drop Solution Calorimetry Data

Cobalt Series

Sample	Drop	Mass (g)		ΔH_{ds} (kJ/mol)	
		Left	Right	Left	Right
$LiCoO_2$	1	5.73	6.35	130.9	129.68
	2	5.00	5.63	129.12	129.34
	3	5.78	5.65	130.12	132.09
	4	6.66	5.52	130.75	129.70
$LiNi_{0.1}Mn_{0.1}Co_{0.8}O_2$	1	5.83	6.01	131.42	130.83
	2	5.69	5.75	131.52	130.23
$LiNi_{0.2}Mn_{0.2}Co_{0.6}O_2$	1	5.58	5.33	129.61	128.77
	2	5.64	5.31	129.04	128.11
$LiNi_{0.25}Mn_{0.25}Co_{0.5}O_2$	1	4.96	4.68	129.81	128.33
	2	5.27	4.58	127.02	127.82
$LiNi_{0.3}Mn_{0.3}Co_{0.4}O_2$	1	5.92	4.98	126.11	125.60
	2	5.64	5.93	126.97	126.54
$LiNi_{0.4}Mn_{0.4}Co_{0.2}O_2$	1	5.55	5.13	122.03	122.07

	2	5.26	5.74	123.02	123.58
$LiNi_{0.5}Mn_{0.5}O_2$	1	5.80	4.77	117.11	115.08
	2	6.84	5.91	117.83	116.63

Drop Solution Calorimetry Data

Nickel Series

Sample	Drop	Mass (g)		ΔH_{ds} (kJ/mol)	
		Left	Right	Left	Right
$LiNiO_2$	1	6.95	4.42	65.14	64.23
	2	4.61	3.50	64.91	64.98
$LiNi_{0.8}Mn_{0.1}Co_{0.1}O_2$	1	5.87	5.63	89.64	91.18
	2	5.30	4.33	90.42	90.56
$LiNi_{0.6}Mn_{0.2}Co_{0.2}O_2$	1	4.18	3.46	100.52	100.67
	2	4.89	4.29	100.56	100.75
$LiNi_{0.5}Mn_{0.25}Co_{0.25}O_2$	1	5.13	3.09	109.55	108.30
$LiNi_{0.4}Mn_{0.3}Co_{0.3}O_2$	1	5.10	3.48	114.29	115.30

	2	6.17	5.55	115.56	115.68
$LiNi_{0.2}Mn_{0.4}Co_{0.4}O_2$	1	5.89	4.07	130.37	129.94
	2	4.21	4.05	128.23	129.11
$LiMn_{0.5}Co_{0.5}O_2$	1	4.11	6.20	144.54	145.87
	2	6.29	5.34	145.31	145.86

Drop Solution Calorimetry Data

Manganese Series

Sample	Drop	Mass (g)		ΔH_{ds} (kJ/mol)	
		Left	Right	Left	Right
Li_2MnO_3	1	4.76	7.97	128.68	129.15
	2	3.48		129.27	
	3	5.34		129.92	
$LiNi_{0.1}Mn_{0.8}Co_{0.1}O_2$	1	6.93	5.48	154.75	155.15
	2	5.71	5.91	154.22	153.14
$LiNi_{0.2}Mn_{0.6}Co_{0.2}O_2$	1	6.65	5.35	140.03	140.50
	2	5.08	5.97	139.45	140.55

$LiNi_{0.25}Mn_{0.5}Co_{0.25}O_2$	1	5.46	6.01	132.46	132.57
	2	5.11	6.35	132.93	133.54
$LiNi_{0.3}Mn_{0.4}Co_{0.3}O_2$	1	4.78	4.63	122.66	124.05
	2	5.57	5.13	123.55	122.65
$LiNi_{0.4}Mn_{0.2}Co_{0.4}O_2$	1	4.59	6.18	107.73	105.52
	2	6.36	5.47	107.47	107.91
$LiNi_{0.5}Co_{0.5}O_2$	1	5.40	7.25	95.28	95.54
	2	3.47	5.41	93.78	93.89